Ataxia-Telangiectasia Mutated Loss-of-Function Displays Variant and Tissue-Specific Differences across Tumor Types

Patrick G. Pilié[1], Virginia Giuliani[2], Wei-Lien Wang[3], Daniel J. McGrail[4], Christopher A. Bristow[2], Natalie Y.L. Ngoi[5], Keith Kyewalabye[1], Khalida M. Wani[3], Hung Le[5], Erick Campbell[5], Nora S. Sanchez[6], Dong Yang[6], Jinesh S. Gheeya[7], Rohit Vivek Goswamy[7], Vijaykumar Holla[6], Kenna Rael Shaw[6], Funda Meric-Bernstam[5,6], Chiu-Yi Liu[2], XiaoYan Ma[2], Ningping Feng[2], Annette A. Machado[2], Jennifer P. Bardenhagen[8], Christopher P. Vellano[2], Joseph R. Marszalek[2], Eeson Rajendra[9], Desiree Piscitello[9], Timothy I. Johnson[9], Maria Likhatcheva[9], Elias Elinati[9], Jayesh Majithiya[9], Joana Neves[9], Vera Grinkevich[9], Marco Ranzani[9], Marina Roy Luzarraga[9], Marie Boursier[9], Lucy Armstrong[9], Lerin Geo[9], Giorgia Lillo[9], Wai Yiu Tse[9], Alexander J. Lazar[3,10], Scott E. Kopetz[11], Mary K. Geck Do[8], Sarah Lively[12], Michael G. Johnson[12], Helen M.R. Robinson[9], Graeme C.M. Smith[9], Christopher L. Carroll[8], M. Emilia Di Francesco[8], Philip Jones[8], Timothy P. Heffernan[2], and Timothy A. Yap[5,6,8]

ABSTRACT

Purpose: Mutations in the *ATM* gene are common in multiple cancers, but clinical studies of therapies targeting ATM-aberrant cancers have yielded mixed results. Refinement of ATM loss of function (LOF) as a predictive biomarker of response is urgently needed.

Experimental Design: We present the first disclosure and preclinical development of a novel, selective ATR inhibitor, ART0380, and test its antitumor activity in multiple preclinical cancer models. To refine ATM LOF as a predictive biomarker, we performed a comprehensive pan-cancer analysis of *ATM* variants in patient tumors and then assessed the *ATM* variant-to-protein relationship. Finally, we assessed a novel ATM LOF biomarker approach in retrospective clinical data sets of patients treated with platinum-based chemotherapy or ATR inhibition.

Results: ART0380 had potent, selective antitumor activity in a range of preclinical cancer models with differing degrees of ATM LOF. Pan-cancer analysis identified 10,609 *ATM* variants in 8,587 patient tumors. Cancer lineage–specific differences were seen in the prevalence of deleterious (Tier 1) versus unknown/benign (Tier 2) variants, selective pressure for loss of heterozygosity, and concordance between a deleterious variant and ATM loss of protein (LOP). A novel ATM LOF biomarker approach that accounts for variant classification, relationship to ATM LOP, and tissue-specific penetrance significantly enriched for patients who benefited from platinum-based chemotherapy or ATR inhibition.

Conclusions: These data help to better define ATM LOF across tumor types in order to optimize patient selection and improve molecularly targeted therapeutic approaches for patients with ATM LOF cancers.

Introduction

The *Ataxia-Telangiectasia Mutated (ATM)* gene is a tumor suppressor frequently mutated in cancer and is involved in multiple cellular processes including DNA damage response (DDR) and cell-cycle regulation (1). The inheritance of two aberrant copies of the *ATM* gene, which results in the autosomal-recessive condition known as ataxia-telangiectasia syndrome, is associated with a significantly elevated lifetime risk of multiple cancer types, including adult-onset epithelial cancers (2). Heterozygous germline variants in *ATM* are seen

[1]Division of Cancer Medicine, The University of Texas MD Anderson Cancer Center, Houston, Texas. [2]TRACTION (Translational Research to Advance Therapeutics and Innovation in Oncology), The University of Texas MD Anderson Cancer Center, Houston, Texas. [3]Department of Pathology, The University of Texas MD Anderson Cancer Center, Houston, Texas. [4]Center for Immunotherapy and Precision Immuno-Oncology, Cleveland Clinic, Cleveland, Ohio. [5]Department of Investigational Cancer Therapeutics (Phase I Program), Division of Cancer Medicine, The University of Texas MD Anderson Cancer Center, Houston, Texas. [6]Institute for Personalized Cancer Therapy, The University of Texas MD Anderson Cancer Center, Houston, Texas. [7]The University of Texas Health Science Center at Houston, Houston, Texas. [8]Institute for Applied Cancer Science, The University of Texas MD Anderson Cancer Center, Houston, Texas. [9]Artios Pharma, the Glenn Berge Building, Babraham Research Campus, Cambridge, United Kingdom. [10]Department of Genomic Medicine, Division of Cancer Medicine, The University of Texas MD Anderson Cancer Center, Houston, Texas. [11]Department of Gastrointestinal Medical Oncology, Division of Cancer Medicine, The University of Texas MD Anderson Cancer Center, Houston, Texas. [12]ChemPartner Corporation, San Francisco, California.

P.G. Pilié and V. Giuliani contributed equally to this article.

T.P. Heffernan and T.A. Yap contributed equally as senior authors of this article.

Corresponding Authors: Timothy A. Yap, Institute for Applied Cancer Science, Investigational Cancer Therapeutics (Phase I Program) and Institute for Personalized Cancer Therapy, The University of Texas MD Anderson Cancer Center, 1400 Holcombe Boulevard, Houston, TX 77030. E-mail: tyap@mdanderson.org; and Timothy P. Heffernan, TRACTION, The University of Texas MD Anderson Cancer Center, 1400 Holcombe Boulevard, Houston, TX 77030. E-mail: TPHeffernan@mdanderson.org

Clin Cancer Res 2024;30:2121–39

doi: 10.1158/1078-0432.CCR-23-1763

Translational Relevance

ATM loss of function (LOF) and its targetability display variant-type and tumor lineage–specific differences, and a novel strategy for using *ATM* LOF as a predictive biomarker that accounts for this heterogeneity can optimize patient selection and improve targeted therapies for patients with cancer.

in 1% to 2% of the population, and individuals with deleterious or inactivating germline variants in *ATM* also carry an increased risk of various types of cancer, including hereditary breast and ovarian cancer (HBOC), prostate cancer, pancreatic cancer, and colorectal cancer, with the strongest evidence for breast cancer (3–7). Somatic variants in *ATM* are frequently found in cancer as well, including in hematologic and solid malignancies. However, the penetrance and cancer phenotypes characterized by somatic *ATM* mutations are less clear than those induced by somatic mutations in DDR genes such as *BRCA1* and *BRCA2 (BRCA1/2)*.

Preclinical studies have shown that cancers with *ATM* LOF are susceptible to DNA-damaging chemotherapies, radiation, and DDR inhibitors, the latter of which includes poly(ADP-ribose) polymerase (PARP) inhibitors (PARPi) and ataxia telangiectasia and Rad3-related protein (ATR) inhibitors (ATRi), in various tissue lineages (8–10). However, clinical studies assessing variants in *ATM* or loss of ATM protein expression (LOP) as a putative predictive biomarker have yielded mixed results. For example, although ATM LOP has retrospectively been shown to predict the benefit of oxaliplatin chemotherapy in patients with colorectal cancer (11), retrospective studies of patients with prostate cancer who received platinum chemotherapy did not show a definitive benefit specific to *ATM* gene aberrations (12). Furthermore, early-phase trials of the PARPi, olaparib, in treating advanced castration-resistant prostate cancer (CRPC) indicated potential clinical benefit in *ATM*-mutant tumors, but these results were not validated in subsequent prospective and retrospective clinical analyses. In contrast, findings from these trials revealed minimal clinical benefit from single-agent PARPi for patients with *ATM* variants (somatic or germline), particularly when compared with CRPC patients harboring *BRCA2* mutations (13–16). Preclinical studies have indicated that *ATM*-null cancers respond to ATRi to a greater degree than to PARPi, with early-phase studies showing durable responses in patients with ATM aberrancy of varying types (8, 17, 18). However, recently reported subsequent expansion trial data of single-agent ATRi in patients with ATM-aberrant cancers have shown heterogeneity in response (19–22).

The performance of *ATM* aberrations as a predictive biomarker in the aforementioned studies is likely hindered by multiple factors. First, the mechanism of ATM in DNA repair is different than BRCA1/2, and therefore the sensitivity to antitumor agents may differ in *ATM*-deficient compared with *BRCA1/2*-deficient tumors. It is also possible that our definition of LOF for some *ATM* variants is inaccurate, and that there is variability in the translation of differing *ATM* mutations to protein function. It is also possible that tumor tissue–specific and zygosity-specific contexts, such as those that have been shown for *BRCA1/2* mutations in predicting response to PARPi (23), may affect the response of *ATM* LOF tumors to anticancer drugs, but this hypothesis has not yet been explored.

Thus, to refine *ATM* LOF predictive biomarker strategies for improved patient selection for rational anticancer therapies, additional research is needed to better understand the biology driving the heterogeneous responses of *ATM* LOF cancers to therapeutic interventions.

In this study, we present the first disclosure and preclinical development of a novel inhibitor of ATR kinase, ART0380, which demonstrates potent and selective antitumor activity in preclinical models with varying types of *ATM* aberrancy. To help resolve the significant heterogeneity in response to anticancer agents, including DDR inhibitors, observed in *ATM* LOF cancers, we performed the largest comprehensive analysis of internal and *in silico* pan-cancer genomic and proteomic data of *ATM* LOF cancers to date. We show that *ATM* variants are found across all solid tumor types as well as span the entirety of the coding sequence of the gene, with relatively few hotspot mutations identified. In addition, our data reveal heterogeneity in *ATM* LOF tumors across patients due to multiple variables, including notable *tissue-specific differences* in (1) the type of variants seen, (2) loss of heterozygosity (LOH), and (3) the relationship between *ATM* variant status and ATM protein expression. This genomic heterogeneity and tissue specificity have significant implications for predictive biomarker development and clinical trial design. We show that factoring in this new information on tissue specificity and combining genomic sequencing with protein IHC for ATM helps clarify the ATM variant-to-protein relationship and identify patients harboring cancers with true ATM LOF that can benefit from specific anticancer therapies.

Materials and Methods

Patient identification

Through a retrospective chart review of the University of Texas MD Anderson Cancer Center (MDACC) internal database and public databases, we identified patients with cancer with at least one *ATM* variant found on clinical genomic sequencing results (Supplementary Fig. S6, consort diagram). Data from The Cancer Genome Atlas (TCGA) samples were acquired from the pan-cancer release from the GDC data portal (https://gdc.cancer.gov/about-data/publications/pancanatlas). Data for additional samples were obtained from cBioPortal at www.cbioportal.org (24–26). Published, existing mutational signatures for TCGA samples were acquired from Knijnenburg and colleagues and analyzed using a generalized regression model (27). Mutation data for additional cohorts were downloaded from cBioPortal.

Gene variant mapping and functional annotation

We mapped variants to their gene location and annotated each variant as inactivating/likely inactivating/VUS/benign based on ACMG 2015 guidelines, using annotation tools as previously published (28–31). Tier 1, or disease-associated variants, were classified as those that are (1) known protein-truncating and inactivating, including frameshift, stop gain, stop loss, or splice variants, and (2) missense variants that are annotated as disease associated in public databases (OncoKB, Human Gene Mutation Database, and/or predicted inactivating/likely inactivating by *in silico* tool InterVar). Tier 2 variants are those that are (1) variants of unknown significance (VUS) or likely benign/benign by the same guidelines. Categorical data (enrichment of mutations in PFAM domains, TP53/ATM comutation, LOH, concordance of LOP with genomic data) were analyzed using Fisher exact test.

ATM IHC

We performed ATM IHC using ATM clone Y170 antibody on 480 tumors (including $N = 263$ patient tumors retrospectively identified from 1,394 tumors with *ATM* variants identified on clinical sequencing, and $N = 217$ tumors prospectively stained for ATM protein

unselected for *ATM* variant status from patients with advanced cancer considering clinical trial enrollment at MDACC. ATM LOP is defined as 100% loss of staining in tumor cell nuclei, with all staining reviewed by a trained pathologist. Analysis of TCGA data was performed by using (−1 × RPPA-derived ATM protein levels) to predict ATM-null variants and are presented as a receiver operating characteristic curve and corresponding area under the curve.

Clinical outcomes in platinum-treated or ATR inhibition treated patients

Through retrospective chart review, we identified 77 patients from the prospectively ATM-stained cohort who had received platinum-based chemotherapy in the metastatic setting with available follow-up data. Progression-free survival (PFS) is displayed using Kaplan–Meier curve for patients with ATM inactivation/loss (Tier 1 variant and/or LOP) versus patients without definitive ATM loss compared using log-rank test. Results were considered statistically significant if $P < 0.05$.

In addition, we identified through chart review 43 patients with *ATM* variants treated on clinical trial(s) at our institution with single-agent ATR kinase inhibition that has previously been reported and had available follow-up data to assess outcomes (20, 21). The study was conducted in accordance with the Declaration of Helsinki and Council for International Organizations of Medical Sciences International Ethical Guidelines, applicable International Conference on Harmonization Good Clinical Practice Guidelines and applicable laws and regulations. All patients provided written informed consent. Clinical benefit rate is defined as stable disease or better for greater than 180 days. PFS is displayed using Kaplan–Meier curve for patients by tumor type using the log-rank test. Results were considered statistically significant if $P < 0.05$.

This study was granted approval by the institutional review board. Data sources and methods are fully described in supplementary materials.

Preclinical methods

ART0380

The synthetic procedures and methods to prepare ART0380 were previously published in the patent application WO2019-014618.

Synthesis of IACS-030106 (*R*-dimethyl ((6-(3-methylmorpholino) -2-(1*H*-pyrrolo[2,3-*b*]pyridin-4-yl)pyrimidin-4-yl)imino)-λ^6-sulfanone; Supplementary Fig. S7).

Step 1. 6(*R*)-4-(2,6-dichloropyrimidin-4-yl)-3-methylmorpholine. To a solution of 2,4,6-trichloropyrimidine (12.3 g, 67.3 mmol/L) and Et_3N (14.2 mL, 101 mmol/L) in EtOH (80 mL) was added (*R*)-3-methylmorpholine (6.8 g, 67 mmol/L). The reaction mixture was stirred at room temperature for 16 hours. The mixture was concentrated under reduced pressure. The residue was diluted with CH_2Cl_2 (200 mL), partitioned with H_2O (150 mL), and the layers were separated. The aqueous layer was extracted with CH_2Cl_2 (3 × 150 mL). The combined organic layers were dried over Na_2SO_4, filtered, and concentrated under reduced pressure. The residue was purified via silica gel chromatography (0%–5% EtOAc in hexanes) to afford the title compound (11.8 g, 71% yield) as a white solid.

Step 2. (*R*)-4-(6-chloro-2-(1H-pyrrolo[2,3-*b*]pyridin-4-yl)pyrimidin- 4-yl)-3-methylmorpholine. A mixture of the product from the previous step (3.0 g, 12 mmol), 4-(4,4,5,5-Tetramethyl-1,3,2-dioxaborolan-2-yl)-1H-pyrrolo[2,3-b]pyridine (2.8 g, 12 mmol), $PdCl_2$(dppf) (0.44 g, 0.60 mmol) and Na_2CO_3 (2.6 g, 24 mmol) in 1,4-dioxane (60 mL) and water (15 mL) was degassed with Ar for 5 minutes. The reaction mixture was heated to 90°C and stirred for 16 hours. The reaction mixture was cooled to room temperature and concentrated under reduced pressure. The residue was purified via silica gel chromatography (0%–50% EtOAc in hexanes) to afford the title compound (1.84 g, 46% yield) as a yellow solid. MS (ES^+) $C_{16}H_{16}ClN_5O$ requires: 329, found: 330 $[M+H]^+$.

Step 3–IACS-030106 (*R*-dimethyl ((6-(3-methylmorpholino)-2-(1*H*-pyrrolo[2,3-*b*]pyridin-4-yl)pyrimidin-4-yl)imino)-λ^6-sulfanone). A reaction vial was charged with the product from the previous step (100 mg, 0.30 mmol), iminodimethyl-λ^6-sulfanone (34 mg, 0.36 mmol; prepared as described below), RuPhos Pd G4 (26 mg, 0.030 mmol), RuPhos (14 mg, 0.030 mmol), Cs_2CO_3 (293 mg, 0.90 mmol), and 1,4-dioxane (2 mL). The vial was purged with N_2 and sealed. The reaction mixture was stirred at 85°C for 16 hours. The reaction mixture was cooled to RT, filtered through CELITE, and concentrated under reduced pressure. The residue was purified by reverse phase preparative HPLC (Mobile phase: A = 10 M NH_4HCO_3/H_2O, B = MeCN; Gradient: B = 20%–50%; 10 minutes; Column: Venusil ASB C18, 10 μm, 150Å, 21.2 mm × 250 mm) to afford the title compound (33.0 mg, 28% yield) as a white solid. ^{1}H NMR (500 MHz, DMSO) δ 11.72 (s, 1H), 8.31 (d, J = 5.0 Hz, 1H), 7.89 (d, J = 5.0 Hz, 1H), 7.59–7.49 (m, 1H), 7.41 (dd, J = 3.3, 1.9 Hz, 1H), 5.92 (s, 1H), 4.45 (s, 1H), 4.06 (d, J = 12.8 Hz, 1H), 3.96 (dd, J = 11.3, 3.4 Hz, 1H), 3.75 (d, J = 11.3 Hz, 1H), 3.64 (dd, J = 11.3, 2.9 Hz, 1H), 3.53–3.47 (m, 1H), 3.45 (s, 6H), 3.15 (td, J = 12.8, 3.8 Hz, 1H), 1.20 (d, J = 6.7 Hz, 3H); MS (ES^+) $C_{18}H_{22}N_6O_2S$ requires: 386, found: 387 $[M+H]^+$.

Synthesis of iminodimethyl-λ^6-sulfanone

To a mixture of benzyl carbamate (2.3 g, 15 mmol), $Rh_2(OAc)_4$ (110 mg, 0.25 mmol), MgO (1.6 g, 40 mmol), and DMSO (780 mg, 10.0 mmol) in CH_2Cl_2 (100 mL) was added $PhI(OAc)_2$ (4.8 g, 15 mmol). The resulting mixture was stirred at RT for 16 h. The reaction mixture was filtered and concentrated under reduced pressure. The residue was purified via flash chromatography (0 – 90% EtOAc in petroleum ether) to afford the title compound (900 mg, 40% yield) as a white solid. MS (ES^+) $C_{10}H_{13}NO_3S$ requires: 227, found: 228 $[M+H]^+$.

A mixture of the product from the previous step (600 mg, 2.6 mmol) and Pd/C (243 mg, 2.6 mmol) was suspended in MeOH (20 mL). The mixture was stirred under an atmosphere of H_2 at 1 atm for 16 h. The reaction mixture was purged with N_2, filtered through CELITE, and the filter pad was washed with MeOH (10 mL). The mixture was concentrated under reduced pressure to afford the title compound (205 mg, 85% yield) as a colorless oil. MS (ES^+) C_2H_7NOS requires: 93, found: 94 $[M+H]^+$.

Synthesis of ART0380 - (*S*)-((2-(2-aminopyridin-4-yl)-6-((*R*)-3-methylmorpholino)pyrimidin-4-yl)imino)(cyclopropyl)(methyl)-λ^6-sulfanone (Supplementary Fig. S8)

Step 1. (*R*)-((2-chloro-6-((*R*)-3-methylmorpholino)pyrimidin-4-yl)imino)(cyclopropyl)(methyl)-λ^6-sulfanone and (*S*)-((2-chloro-6-((*R*)-3-methylmorpholino)pyrimidin-4-yl)imino)(cyclopropyl)(methyl)-λ^6-sulfanone. To a solution of (*R*)-4-(2,6-dichloropyrimidin-4-yl)-3-methylmorpholine (synthesized as described for IACS-030106; 22 g, 0.19 mol) and cyclopropyl(imino)(methyl)-λ^6-sulfanone (47 g, 0.19 mol/L; prepared as described below) in dioxane (750 mL) were added $Pd_2(dba)_3$ (8.6 g, 9.4 mmol/L), XantPhos (5.5 g, 9.4 mmol/L) and Cs_2CO_3 (184 g, 0.57 mol/L) and the resulting mixture was purged with N_2 (3×), heated to 80°C and stirred under an

atmosphere of N_2 for 6 hours. The reaction mixture was cooled to room temperature, filtered through CELITE, and concentrated under reduced pressure. The residue was purified via silica gel chromatography (0%–100% EtOAc in hexanes) to afford the title compounds as a mixture of diastereomers (26 g, 41% yield) as an off-white solid. A solution of the mixture of diastereomers (35 g, 0.11 mol) in CH_2Cl_2 (300 mL) was separated by Chiral SFC (Mobile phase: CO_2/EtOH = 75/25; Flow rate: 70 g/minute; 4 minutes; Column temperature: 35°C; Back pressure: 100 bar; Column: Daicel CHIRALPAK AD, 10 μm, 20 mm × 250 mm) to afford **Isomer 1a** (15.0 g, 86%) as a light yellow solid and **Isomer 1b** (14.2 g, 81%) as a light yellow solid. **Isomer a** ((*R*)-cyclopropyl(methyl)-λ^6-sulfanone or (*S*)-cyclopropyl(methyl)-λ^6-sulfanone): ^{1}H NMR (400 MHz, $CDCl_3$) δ 5.69 (s, 1H), 4.15–4.05 (m, 1H), 3.93–3.79 (m, 2H), 3.67 (d, *J* = 11.5 Hz, 1H), 3.59 (app. d, *J* = 11.5 Hz, 1H), 3.51–3.39 (m, 1H), 3.36 (s, 3H), 3.12 (td, *J* = 12.8, 3.4 Hz, 1H), 2.87–2.76 (m, 1H), 1.51–1.40 (m, 1H), 1.28–1.21 (m, 1H), 1.19 (d, *J* = 6.7 Hz, 3H), 1.14–0.99 (m, 2H); MS (ES^+) $C_{13}H_{19}ClN_4O_2S$ requires: 330, found: 331 $[M+H]^+$; R_t = 3.19 minutes. **Isomer b** ((*R*)-cyclopropyl(methyl)-λ^6-sulfanone or (*S*)-cyclopropyl(methyl)-λ^6-sulfanone): ^{1}H NMR (400 MHz, $CDCl_3$) δ 5.68 (s, 1H), 4.14–4.05 (m, 1H), 3.88 (dd, *J* = 11.5, 3.9 Hz, 1H), 3.83 (d, *J* = 13.6 Hz, 1H), 3.67 (d, *J* = 11.5 Hz, 1H), 3.59 (dd, *J* = 11.5, 3.2 Hz, 1H), 3.45 (td, *J* = 11.9, 3.1 Hz, 1H), 3.37 (s, 3H), 3.12 (td, *J* = 12.8, 3.9 Hz, 1H), 2.81 (ddd, *J* = 12.8, 8.0, 4.8 Hz, 1H), 1.49–1.41 (m, 1H), 1.27–1.20 (m, 1H), 1.18 (d, *J* = 6.8 Hz, 3H), 1.14–1.01 (m, 2H); MS (ES^+) $C_{13}H_{19}ClN_4O_2S$ requires: 330, found: 331 $[M+H]^+$; R_t = 5.62 minutes.

Step 2. ART0380 - (*S*)-((2-(2-aminopyridin-4-yl)-6-((*R*)-3-methylmorpholino)pyrimidin-4-yl)imino)(cyclopropyl)(methyl)-λ^6-sulfanone. A microwave vial was charged with a 0.05 mol/L solution of Isomer b (1.0 eq) in a 3:1 mixture of dioxane/H_2O v/v, and 4-(4,4,5,5-tetramethyl-1,3,2-dioxaborolan-2-yl)pyridin-2-amine (2.0 eq), Na_2CO_3 (6.0 eq), Pd(dppf)Cl_2 (0.14 eq) were added. The vial was purged with N_2 and sealed. The reaction mixture was heated at 80°C for 3 hours. The reaction mixture was cooled to room temperature, filtered through CELITE, and concentrated under reduced pressure. The residue was purified by reverse phase preparative HPLC (Mobile phase: A = 10 mmol/L NH_4HCO_3/H_2O, B = MeCN; Gradient: B = 25–55%; 18 minutes; Column: Welch XB-C18, 10 μm, 150Å, 21.2 mm × 250 mm) to afford the title compound as a white solid. ^{1}H NMR (500 MHz, CD_3OD) δ 8.03–7.91 (m, 1H), 7.53 (s, 1H), 7.49 (dd, *J* = 5.5, 1.4 Hz, 1H), 5.97 (s, 1H), 4.48 (d, *J* = 4.6 Hz, 1H), 4.11 (d, *J* = 12.0 Hz, 1H), 4.02 (dd, *J* = 11.3, 3.6 Hz, 1H), 3.82 (d, *J* = 11.4 Hz, 1H), 3.75 (dd, *J* = 11.5, 3.0 Hz, 1H), 3.65–3.56 (m, 4H), 3.25 (td, *J* = 12.8, 3.8 Hz, 1H), 3.01 (td, *J* = 7.9, 4.0 Hz, 1H), 1.42 (dd, *J* = 10.2, 5.4 Hz, 1H), 1.31 (dd, *J* = 11.1, 6.2 Hz, 4H), 1.20 (dt, *J* = 11.3, 5.7 Hz, 2H); MS (ES^+) $C_{18}H_{24}N_6O_2S$ requires: 388, found: 389 $[M+H]^+$; R_t = 11.35 minutes.

Synthesis of cyclopropyl(imino)(methyl)-λ^6-sulfanone

To a solution of 1-bromo-4-(methylsulfinyl)benzene (10.5 g, 48.0 mmol/L) in THF (100 mL) was added cyclopropylmagnesium bromide (1M, 72 mL, 72 mmol/L) at 0°C slowly. The mixture was stirred at 0°C for 1.5 hours. Saturated aqueous NH_4Cl was added (200 mL), the layers were separated, and the aqueous layer was extracted with CH_2Cl_2 (5 × 150 mL). The combined organic layers were dried over Na_2SO_4, filtered, and concentrated under reduced pressure. The residue was purified via flash chromatography (50%–100% EtOAc in petroleum ether) to afford the title compound (3.2 g, 64% yield) as a yellow oil. MS (ES^+) C_4H_8OS requires: 104, found 105 $[M+H]^+$. To the solution of the product from the previous step (22 g, 0.21 mol) and $PhI(OAc)_2$ (204 g, 0.64 mol) in MeOH (100 mL) at 0°C was added NH_3 (120 mL, 0.84 mol, 7 N in MeOH) dropwise. The resulting mixture was allowed to warm to room temperature and stirred for 2 hours. The reaction mixture was concentrated under reduced pressure. The residue was purified via flash chromatography (15% EtOAc in petroleum ether, then with 2% MeOH in CH_2Cl_2) to afford the title compound (20 g, 79%) as a yellow oil: ^{1}H NMR (400 MHz, CDCl3) δ 3.06 (s, 3H), 2.58 (tt, J = 7.9, 4.8 Hz, 1H), 1.26–1.19 (m, 1H), 1.19–1.12 (m, 1H), 1.05 (dt, J = 11.1, 4.5 Hz, 2H).

ATR/ATRIP enzymatic assay

Human full-length FLAG-TEV-ATR and His_6-ATRIP were coexpressed in HEK293 cells. The cell pellet (20 g) was harvested and lysed in 100 mL of lysis buffer (20 mmol/L Tris-HCl pH 7.5 at room temperature, 137 mmol/L NaCl, 10% glycerol, 1 mmol/L DTT, 1% (v/v) Tween-20, 0.1% (v/v) NP-40, complete protease inhibitor cocktail tablets, phosphatase inhibitor cocktail tablets, 2 mmol/L $MgCl_2$, 0.2 mmol/L EDTA, and 1 mmol/L ATP). After sonication and centrifugation, the supernatant was incubated at 4°C for 3 hours with 1 mL of anti-FLAG resin (Sigma-Aldrich catalog no. A2220) that had been preequilibrated in buffer A (20 mmol/L Tris-HCl pH 7.5 at room temperature, 137 mmol/L NaCl, 10% glycerol, 1 mmol/L DTT, 2 mmol/L $MgCl_2$, and 0.2 mmol/L EDTA). The sample was loaded into a column, and then washed with buffer A three times. Protein was subsequently eluted with 2 mL of buffer B (buffer A + 200 μg/mL 3 × FLAG peptide). The ability of new chemical matter to inhibit the ATR catalytic activity in this ATR/ATRIP complex was assessed using a Caliper-based assay. A 2× enzyme solution (i.e., 4 nmol/L enzyme) was prepared using 1× Kinase Reaction Buffer (25 mmol/L HEPES pH 8, 0.0055% Brij-35, 10 mmol/L $MnCl_2$, and 1 mmol/L DTT). A 2× peptide solution was then prepared consisting of 10 μmol/L FAM-labeled RAD17 peptide (GL Biochem, catalog no. 524315) in 1× Kinase Reaction Buffer supplemented with 2 μmol/L ATP. Ten microliters of the 2× enzyme solution was transferred to an assay plate containing 60 nL of test compound (from a 3× serial dilution) in 100% DMSO. Following a 30-minute incubation at 28°C, 10 μL of the 2× peptide solution was then transferred to the same assay plate. The reaction was allowed to incubate at 28°C for 6 hours. After adding 30 μL of stop buffer (100 mmol/L HEPES pH 7.5, 0.015% Brij-35, 0.2% Coating-3 Regeant; PerkinElmer, catalog no. PN760050), and 50 mmol/L EDTA), data were collected on a Caliper instrument. Conversion values were converted to inhibition values via the following equation: % inhibition = (max − conversion)/(max − min) × 100, whereby "max" corresponds to the DMSO control and "min" corresponds to the low control. IC_{50} values were calculated using the following equation in XLFit: Y = Bottom + (Top − Bottom)/1 + $(IC_{50}/X)^{HillSlope}$).

Cell-based assays

Inhibitors of ATR kinase are effective at inhibiting the ATR-driven phosphorylation of the downstream target Chk1 (CHEK1) kinase at serine 345, following the addition of 4-nitroquinoline N-oxide, a chemical used to induce DNA damage. Cellular EC_{50} for the inhibitors of ATR described herein were measured in HT-29 colorectal adenocarcinoma cells. HT-29 cells were routinely maintained in McCoy's 5A media (ATCC catalog no. 30-2007) supplemented with 10% fetal bovine serum (Sigma-Aldrich, catalog no. F2442) and 1× penicillin–streptomycin (Gibco, catalog no. 15140-122) using a humidified incubator (37°C, 5% CO_2, and ambient O_2). In preparation for the CHK1 (p-Ser345) ALPHASCREEN SUREFIRE assay, cells were harvested and resuspended in McCoy's 5A media supplemented with 10% fetal bovine serum and 1× penicillin–streptomycin. Cells were seeded

onto a 384-well black CELLSTAR tissue culture plate (VWR, catalog no. 89085-314) at a density of 13,000 cells/well in a volume of 40 μL. The microplate was incubated overnight (approximately 20 hours) at 37°C with 5% CO_2 and ambient O_2. Stock solutions of the test compounds were prepared in 100% DMSO (Sigma-Aldrich, catalog no. D2650) and serially diluted 1:3 using 100% DMSO. Compounds were additionally diluted 1:33 in culture medium, and 10 μL/well was transferred to the tissue culture plate. Following the compound addition, the microplate was incubated at 37°C for 90 minutes. Ten microliters of 4-nitroquinoline N-oxide (Sigma-Aldrich, catalog no. N8141-1G) diluted in media (final concentration 12 μmol/L) was added to the tissue culture plate followed by a 120-minute incubation at 37°C. The cells were then washed with PBS and lysed using 10 μL/well SUREFIRE Kit lysis buffer diluted to 1× in water (PerkinElmer, catalog no. TGRCHK1S50K), with mixing on an orbital shaker at 500 rpm for 20 minutes at room temperature. Lysates were frozen at −20°C overnight. Four microliters/well of lysate was then transferred from the tissue culture plate to a 384-well, white, low volume, PROXIPLATE (PerkinElmer, catalog no. 600828). Five microliters/well of the acceptor bead solution, prepared by diluting SUREFIRE Kit activation buffer (PerkinElmer, catalog no. TGRCHK1S50K) and ALPHASCREEN Protein A acceptor beads (PerkinElmer, catalog no. 6760617R) in SUREFIRE Kit reaction buffer (PerkinElmer, catalog no. TGRCHK1S50K), was added to the lysates under subdued light and incubated at room temperature for 120 minutes. Two microliters/well of the donor bead solution, prepared by diluting ALPHASCREEN Streptavidin donor beads (PerkinElmer, catalog no. 6760617R) in SUREFIRE Kit dilution buffer (PerkinElmer, catalog no. TGRCHK1S50K), was added under subdued light and incubated at room temperature for an additional 120 minutes. The pCHK1 ALPHASCREEN signal was measured using an Envision plate reader (PerkinElmer). EC_{50} values were calculated using a four-parameter logistic curve fit using Genedata Screener software. The percentage of control for each compound concentration was calculated by the following formula: 100 × (Compound − Min)/(Max − Min) where "Max" is the high control, DMSO, and "Min" is the low control, 5 μmol/L ATR inhibitor.

Cellular selectivity was evaluated with the inhibition of phospho-ribosomal protein S6 (Ser235/236) using an In-Cell Western assay. HT-29 cells were cultured and compounds were diluted as described above. Cells were seeded onto a 384-well, black, clear bottom, poly-D-lysine coated tissue culture plate (Greiner, catalog no. 781946) at a density of 1500 cells/well in a volume of 50 μL. After an overnight incubation, cells were treated with compounds at 37°C for 2 hours. Cells were fixed and permeabilized before addition of 20 μL/well of p-RPS6 (Ser235/236) antibody (Cell Signaling, catalog no. 2211) and then incubated for 1 hour at room temperature. Cells were washed with 1X PBST, 20 μL/well of 1:500 CellTag 700 Stain (LI-COR, catalog no. 926-41090) and 1:1000 of IRDye 800CW goat anti-rabbit IgG secondary antibody (LI-COR, catalog no. 926-32211) were added, and the plate was incubated at room temperature for 1 hour. After a final wash, the LI-COR Odyssey Imager was used to measure the signal. The CellTag 700 was used to normalize the p-RPS6 signal and EC_{50} values were calculated using a four-parameter logistic curve fit using Genedata Screener software.

In vitro cellular proliferation assay

NCI-H23 (ATCC, no. CRL-5800, RRID:CVCL_1547) cells were purchased from the ATCC and routinely maintained in RPMI medium 1640 containing 2 mmol/L L-glutamine (Gibco, catalog no. 11875-093) supplemented with 10% fetal bovine serum (Sigma-Aldrich, catalog no. F2442), 100 units/mL penicillin and 100 μg/mL streptomycin (Gibco, catalog no. 15140-122) in a humidified incubator (37°C, 5% CO_2). Prior to the assay, cells were harvested and seeded onto a 384-well, white tissue culture plate (PerkinElmer, catalog no. 6007680) at a density of 200 cells/well in a volume of 50 μL. The tissue culture plate was incubated for 24 hours at 37°C with 5% CO_2. Stock solutions of the test compounds were prepared in 100% DMSO (Sigma-Aldrich, catalog no. D2650) and serially diluted 1:3 using 100% DMSO. Compounds were additionally diluted 1:40 in the culture medium, and 10 μL/well was transferred to the tissue culture plate. Following the compound addition, the microplate was incubated at 37°C. After 7 days, viability was assessed with the addition of 30 μL of CellTiter-Glo 2.0 (Promega, catalog no. G9243). The tissue culture plate was then shaken on an orbital shaker at 300 RPM for 10 minutes at room temperature in the dark. Luminescence was measured using a PerkinElmer Envision plate reader. EC_{50} values were calculated using a four-parameter logistic curve fit using Genedata Screener software. CCD-18Co (ATCC, no. CRL-1459) cells were purchased from ATCC and routinely maintained in EMEM (ATCC, catalog no. 30-2003) supplemented with 10% fetal bovine serum (Sigma-Aldrich, catalog no. F2442), 100 units/mL penicillin and 100 μg/mL streptomycin (Gibco, catalog no. 15140-122) in a humidified incubator (37°C, 5% CO_2). Prior to the assay, cells were harvested and seeded onto a 384-well, white tissue culture plate (PerkinElmer, catalog no. 6007680) at a density of 200 cells/well in a volume of 50 μL. All other details of the procedure were identical to those described above for the NCI-H23 cells. Granta-519 (catalog no. ACC 342) cells were purchased from DSMZ and routinely maintained in DMEM (Gibco, catalog no. 10564–011) supplemented with 10% heat-inactivated fetal bovine serum (Gibco, catalog no. 16140-071), 100 units/mL penicillin and 100 μg/mL streptomycin (Gibco, catalog no. 15140-122) in a humidified incubator (37°C, 5% CO_2). Prior to the assay, cells were harvested and seeded onto a 384-well, white tissue culture plate (PerkinElmer, catalog no. 6007680) at a density of 400 cells/well in a volume of 50 μL. All other details of the procedure were identical to those described above for the NCI-H23 cells. LoVo (catalog no. CCL-229) cells were purchased from ATCC and routinely maintained in F12K (ATCC, catalog no. 30-2004) supplemented with 10% fetal bovine serum (Sigma-Aldrich, catalog no. F2442), 100 units/mL penicillin and 100 μg/mL streptomycin (Gibco, catalog no. 15140-122) in a humidified incubator (37°C, 5% CO_2). Prior to the assay, cells were harvested and seeded onto a 384-well, white tissue culture plate (PerkinElmer, catalog no. 6007680) at a density of 200 cells/well in a volume of 50 μL. All other details of the procedure were identical to those described above for the NCI-H23 cells.

NCI-H460 (ATCC, catalog no. HTB-177) cells were purchased from the ATCC and routinely maintained in RPMI medium 1640 containing stable glutamine and 2 g/L $NaHCO_3$ (PAN-Biotech, catalog no. P04-18500) supplemented with 10% fetal bovine serum (PAN-Biotech, catalog no. P30-3306) in a humidified incubator (37°C, 5% CO_2). Calu-6 (ATCC, catalog no. HTB-56) cells were purchased from the ATCC and routinely maintained in advance EMEM Medium (Gibco, catalog no. 12492-013) supplemented with 1X GlutaMAX (Gibco, catalog no. 35050-038) and with 10% fetal bovine serum (PAN-Biotech, catalog no. P30-3306) in a humidified incubator (37°C, 5% CO_2). PC-3 (ATCC. catalog no. CRL-1435, RRID:CVCL_0035) cells were purchased from the ATCC and routinely maintained in Ham's F-12K (Kaighn's) medium (Gibco, catalog no. 21127022) supplemented with 10% fetal bovine serum (PAN-Biotech, catalog no. P30-3306) in a humidified incubator (37°C, 5% CO_2).

NCI-H460 (RRID:CVCL_0459) parental and ATM KO cells were harvested and seeded onto a 96-well, white tissue culture plate (VWR, catalog no. 734-1610) at a density of 150 cells/well in a volume of 150 μL. The tissue culture plate was incubated for 24 hours at 37°C with 5% CO_2. Stock solutions of the test compounds were prepared in 100% DMSO (Apollo Scientific, catalog no. BID1200) and serially diluted 1:3 using culture media containing 0.7% DMSO. Twenty-five microliters/well was transferred to the tissue culture plate (1:7 dilution). Following the compound addition, the microplate was incubated at 37°C.

Calu-6 and PC-3 isogenic cell lines were harvested and seeded onto a 96-well, white tissue culture plate (VWR, catalog no. 734-1610) at a density of 1,200 cells/well for Calu-6, 1,000 cells/well for PC-3, and 3,000 cells/well for PC-3 ATM KO. Plates were treated with stock solutions of the test compounds prepared in 100% DMSO (Apollo Scientific, catalog no. BID1200) using Tecan D300e Digital Dispenser. Following the compound addition, the microplate was incubated at 37°C.

After 7 to 10 days, viability was assessed with the addition of 50 μL of CellTiter-Glo 2.0 (Promega, catalog no. G7573). The tissue culture plate was then shaken on an orbital shaker at 450 RPM for 4 minutes at room temperature. Luminescence was measured using the CLARIOstar plate reader after 30 minutes of incubation at room temperature. Viability data for each compound were plotted as a percentage of viability normalized against DMSO, and EC_{50} values were calculated using a four-parameter logistic curve fit using GraphPad Prism software.

Generation of ATM KO isogenic models

NCI-H460 ATM KO clones were generated by Oxford Genetics. Briefly, synthetic guide RNAs (sgRNA) for CRISPR/Cas9 were designed to specifically target exon 34 of the ATM gene (reference transcript ENST00000675843.1). The 5′→3′ sequence of the sgRNA target used is: GACCTACCTGAATAACACAC. Pools of cells carrying the edited gene were generated by transient cotransfection of the sgRNA complexed with CRISPR/Cas9 protein. Single cells were isolated, and the targeted exon was sequenced by Sanger sequencing. Selected clones with out-of-frame insertion/deletions in all alleles were expanded and validated by PCR followed by high-throughput sequencing. The NCI-H460 ATM KO clone was characterized as carrying an out-of-frame deletion causing the expected loss of protein expression. Loss of protein expression was confirmed by Western blot.

Following a similar experimental approach, PC-3 and Calu-6 ATM KO clones were generated by Oxford Genetics and by Synthego, respectively, using sgRNA targeting exon 3 of ATM with 5′→3′ sequence CGGCAUUCAGAUUCCAAACA), and were validated as described above.

Immunofluorescence and quantitative image-based cytometry

Cells were seeded at a density of 8,000 cells per well in 100 μL of media in 96-well collagen coated plates (Revvity, catalog no. 6055700). Following 24 hours of a dose titration of ART0380 treatment, media were replenished with media with or without drug for an additional 24 hours. Cells were labeled with 10 μmol/L EdU (5-Ethynyl-2′-deoxyuridine) for the last 30 minutes, washed with PBS, and fixed in 4% paraformaldehyde (ChemCruz, catalog no. sc-281692) for 10 minutes at room temperature. Cells were then washed twice with PBS and permeabilized and blocked in 0.5% Triton/0.5% BSA 1× PBS for 30 minutes and processed using the Click-iT EdU Alexa Fluor 647 Flow cytometry Kit (Life Technologies, catalog no. C10340) according to the manufacturer's instruction. Then, antibody labeling was performed using primary antibodies against γH2AX and GEMININ (Millipore, catalog no. 05-636, 1:2,000; Abcam, catalog no. ab195047, RRID:AB_2832993, 1:1,000, respectively) overnight at 4°C. Cells were then washed twice in 0.1% Triton/1× PBS, followed by secondary antibody staining (Invitrogen, catalog no. A11004 and A11034, RRID: AB_2576217, 1:2,000) and DAPI counterstain (1 mg/mL, Thermo Fisher Scientific, catalog no. 62248) for 1 hour at room temperature. Plates were imaged on Operetta CLS (Revvity) using a 20× air objective. γH2AX foci quantification and cell-cycle analysis were performed using Harmony V4.9 within a nuclear mask generated from DAPI staining.

Annexin V/propidium iodide staining

Cells were seeded at a density of 4×10^5 cells per well in 2 mL of media in 6-well plates (Corning Costar, catalog no. 3506). Cells were then treated with a dose titration of ART0380 for 24 hours or 48 hours. Cells were processed using the dead cell Apoptosis Kit with Annexin V (Life Technologies, catalog no. V13242) according to the manufacturer's instruction.

Western blot

Cells were lysed in RIPA (radioimmunoprecipitation assay) buffer (Thermo Fisher Scientific, catalog no. 89901) supplemented with protease and phosphatase inhibitors (Thermo Fisher Scientific, catalog no. 78440), 4.5 mmol/L $MgCl_2$ (Sigma-Aldrich, catalog no. M1028) and Benzonase nuclease (Sigma-Aldrich, catalog no. E1014). Whole-cell lysates were separated on 3% to 8% Tris-Acetate NuPAGE gels (Thermo Fisher Scientific, catalog no. EA037) and analyzed by standard immunoblotting. The following primary antibodies were used: SMG1 (catalog no. 9149S, 1:1,000), pS6 (pRPS6) S240/244 (catalog no. 5364, 1:1,000), S6 (RPS6) (catalog no. 2317, RRID:AB_2238583, 1:1,000), pmTOR (pMTOR) S2448 (catalog no. 5536, 1:1,000), mTOR (MTOR) (catalog no. 4517, 1:1,000), pP70-S6K (pRPS6KB1) T389 (catalog no. 9206, 1:1,000), P70-S6K (RPS6KB1) (catalog no. 2708, 1:1,000), ATM (Cell Signaling Technology, catalog no. 92356, 1:500), pATR T1989 (catalog no. 30632, no. 58014 1:1,000), pCHK1 (pCHEK1) S345 (catalog no. 2341, 1:1,000), pCHK2 (pCHEK2) T68 (catalog no. 2197, 1:1,000), CHK2 (CHEK2) (catalog no. 3440, 1:1,000), pUPF1 S1107 (catalog no. 84283, 1:1,000), UPF1 (catalog no. 12040, 1:1,000), GAPDH (catalog no. 3683, 1:1,000), H2AX (catalog no. 7631, 1:1,000), β-Tubulin (TUBB) (catalog no. 86298, 1:1,000) from Cell Signaling Technology. Kap1 (TRIM28) (ab22553, 1:1,000), Kap1 (TRIM28) pS824 (ab243870, 1:1,000), p-DNA-PKcs (pPRKDC) S2056 (catalog no. 18192, 1:1,000), p-ATM S1981 (catalog no. 81292, 1:1,000) from Abcam. DNA-PKcs (PRKDC) (catalog no. 5282, 1:1,000), Vinculin (catalog no. 73614, 1:1,000) from Santa Cruz Biotechnology. γH2AX (catalog no. 05-636, 1:1,000), ATR (catalog no. sc515173, 1:1,000), ATR (catalog no. MA123158, 1:1,000), CHK1 (CHEK1) (catalog no. C9358, 1:1,000), ATM (catalog no. 07-1286, 1:500) from Merck/Sigma-Aldrich.

The following secondary antibodies were used: goat anti-mouse IgG (H+L) Secondary Antibody HRP (catalog no. 31430, RRID: AB_228307, 1:10,000) and goat anti-rabbit IgG (H+L) Secondary Antibody HRP (catalog no. 31460, RRID:AB_228341, 1:10,000) from Thermo Fisher Scientific; IRDye 800CW goat anti-rabbit IgG Secondary Antibody (catalog no. 926-32211, 1:15,000) and IRDye 680CW goat anti-mouse IgG Secondary Antibody (catalog no. 926-68070, 1:15,000) from LI-COR Odyssey M. Immunoblots are representative of experiments that were performed at least twice.

In vivo studies

All *in vivo* work was approved by the IACUC of the MDACC. For LoVo and Granta-519 xenograft studies, female CD-1 nude (Charles River Laboratories) or female NSG (The Jackson Laboratory), respectively, between 6 and 12 weeks old were used as recipients. Cells were harvested, counted, and resuspended at 1 million cells/100 μL in PBS. Cell suspension was mixed 1:1 with Matrigel and a total volume of 200 μL/mouse was injected subcutaneously in the right flank of immune-compromised mice.

Tumor growth was monitored with caliper and tumor volume (TV) calculated using a standard formula: (length × width^2)/2. Mice were allocated to different groups according to their TV (between 150 and 250 mm^3) to give homogeneous mean and median TV in each treatment arm. Treatments were randomly attributed, and mice were treated as indicated for each study. The tolerability of the tested compound was evaluated by clinical sign observation and body weight measurement during treatment.

Colorectal cancer patient–derived xenografts (PDX) were developed by patient-derived samples obtained from consented patients under an institutional review board (IRB)–approved protocol LAB10-0982, chaired by S.K. (UTMDACC) and kindly provided by Dr. Scott Kopetz (MDACC). ATM gene mutation status for PDX is listed in Supplementary Table S1. For PDX studies, tumor fragments were transplanted subcutaneously in NSG mice. When tumors reached between 150 and 250 mm^3, mice were randomized into experimental groups as indicated for each study. Treatment response was determined by percent tumor growth inhibition (%TGI), defined as the percent difference between final median tumor volumes of treated and control groups.

Western blot analysis of pChk1ser345 in tumor lysates

Snap-frozen tumor sections (10–20 mg) were blended and lysed at 4°C in RIPA buffer using Bullet Blender. After 30 minutes of incubation at 4°C, homogenized tissue was spun at 14,000 rpm for 15 minutes at 4°C. The supernatant was collected and protein was quantified using BCA assay. About 40 μg of protein was loaded into a 4% to 12% SDS-PAGE gel and transferred to a nitrocellulose membrane. After 1 hour of blocking at room temperature with 5% skim milk, membrane was incubated with primary antibody pChk1ser345 (Cell Signaling Technology, no. 2348, Rabbit mAb) at 1:500 dilution in 5% BSA/PBST buffer overnight at 4°C. After washing with PBST, the membrane was incubated for 1 hour at room temperature with goat-anti-rabbit-HRP secondary antibody (Cell Signaling Technology, no. 7074S, 1:1,000 dilution in 5% milk) and then immunoreactive protein bands were visualized by ECL kit (SuperSignal West Femto, Thermo Fisher Scientific, no. PI34095) using ImageQuant (RRID:SCR_014246). Image Studio software was used to quantify the signals.

Multiplexed immunofluorescence staining and data analysis

Formalin-fixed and paraffin-embedded (FFPE) colorectal cancer PDX samples were sectioned into 3-μm-thick sections and placed on positively charged slides. Sections were deparaffinized by baking at 60°C for 1 hour, then rehydrated by serial passage through xylene and graded alcohol. All sections were subjected to an initial heat-induced epitope retrieval (HIER) in Tris-EDTA buffer, pH 9.0 (ab93684), at 95°C for 30 minutes using a BioGenex EZ retrieval microwave. Subsequent HIER for Opal development was done using fresh citrate buffer at 95°C for 10 minutes. All sections were initially blocked for endogenous peroxidase using Bloxal (Vector Labs SP6000). After and before each primary incubation, sections were blocked using 2.5% Natural Goat serum (Vector Labs S1012). Opal and direct immunofluorescence methods were used. ATM (Ab32420 1/2000) was developed using Opal method. HLA-A conjugated to Alexa 647 (Abcam 199837, at 1/500) was used to aid in tissue segmentation. Sections were then counterstained with DAPI.

Slides were imaged using Vectra 3.0 Automated Quantitative Pathology Imaging System (Akoya Biosciences). Image processing and analysis was performed using inForm Software v2.4 (Akoya Biosciences). For a subset of images from each PDX, the following was performed: Images were unmixed, and autofluorescence was removed. Then, tissue was segmented as tumor, stroma, or other based on training regions and pattern recognition of DAPI and HLA-A stain. This was followed by cell segmentation using DAPI and HLA-A to segment nuclei, cytosol, and membrane. Phenotyping was performed for each marker individually by selecting representative positives for algorithm training and allowing the software to select the rest. Batch analysis of all images was performed using the segmentation and phenotyping algorithm described above. Data analysis was performed using phenoptrReports (Akoya Biosciences), an R script package. Briefly, all single-cell phenotype data were merged, aggregated, and consolidated for each marker. Consolidated data were analyzed based on the phenotypes of interest. All data were graphed using GraphPad Prism v 8.0.

Data availability

Through IRB-approved, retrospective chart review of the University of Texas MD Anderson Cancer Center (MDACC) internal database (MOCLIA), patients with DNA variants in ATM gene were identified from clinical genomic sequencing results. De-identified ATM variant information from internal clinical sequencing results and more detailed PDX mutation data beyond ATM mutations can be obtained upon request from the corresponding authors. Additional data used for analysis are all publicly available for download (Supplementary Table S1). Data from TCGA samples were acquired from the pan-cancer atlas release and are available at the Genomic Data Commons (https://gdc.cancer.gov/about-data/publications/pancanatlas). Molecular data for additional patient samples were obtained from publicly available cohorts deposited on cBioPortal (www.cbioportal.org) and AACR Genie Project (https://www.synapse.org/#!Synapse:syn7222066 and https://genie.cbioportal.org) as referenced (24, 26). Established, published mutational signatures were analyzed from publicly available sequencing data for TCGA samples using a generalized regression model (27, 32, 33).

Results

ATM-deficient cells of varying types are sensitive to ART0380, a novel and potent inhibitor of ATR kinase activity

Herein, we introduce ART0380, a novel, potent, and selective orally bioavailable inhibitor of ATR kinase currently in phase I clinical testing in patients with advanced or metastatic solid cancers (**Fig. 1A**; NCT04657068). ART03080 was identified through an extensive lead optimization campaign and selected for clinical development on the basis of its excellent physicochemical and pharmacokinetic (PK) properties as well as compelling *in vitro* and *in vivo* pharmacologic profiles (**Fig. 1**). ART0380 is an ATP-competitive inhibitor that binds in the ATP pocket of ATR, occupying the same space where ATP would bind by engaging the hinge with the morpholine oxygen and filling the ribose pocket with the sulfoximine group. Biochemical characterization showed that ART0380 is a potent inhibitor of the

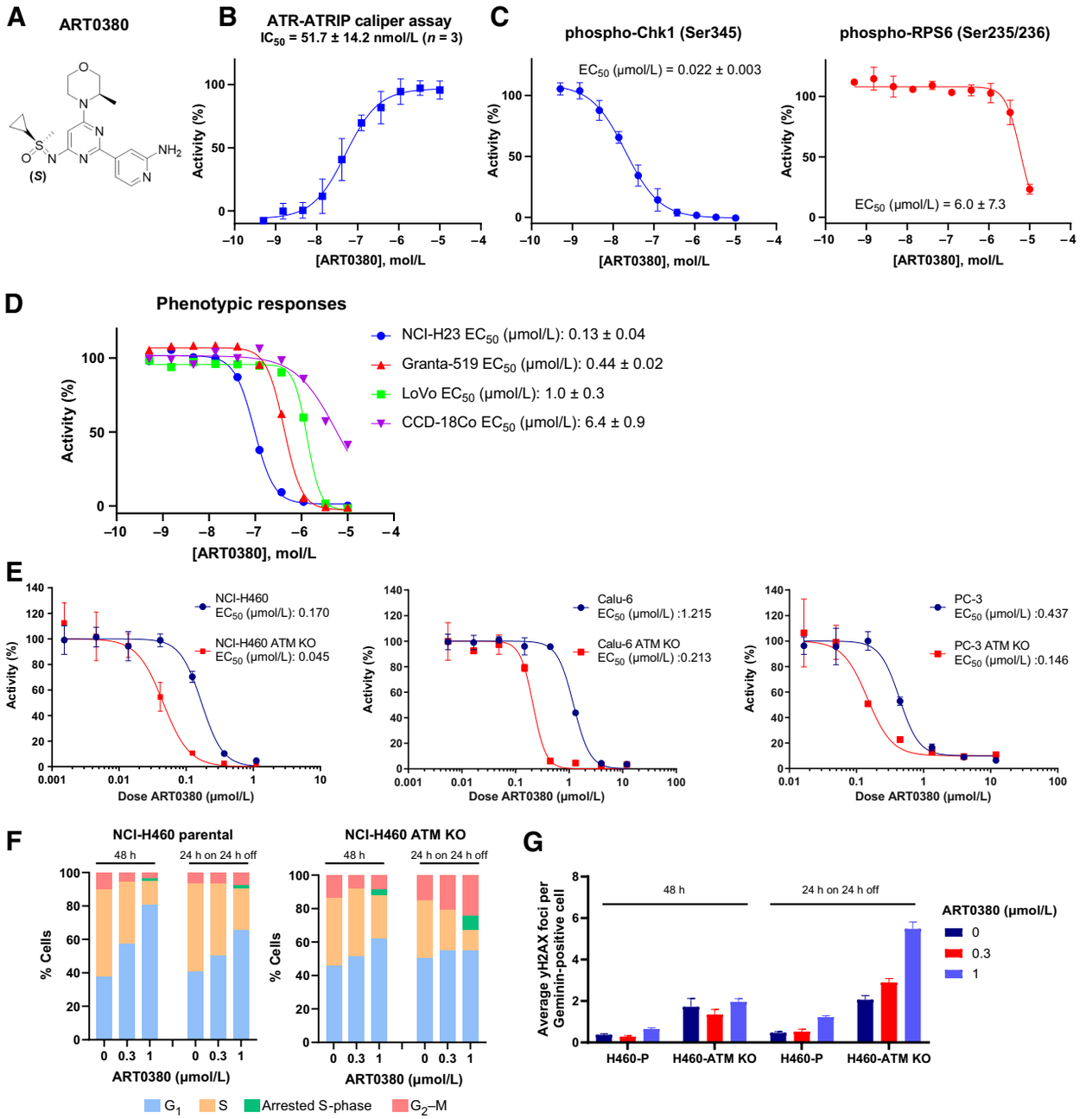

Figure 1.

ART0380 is a potent and selective ATR inhibitor (ATRi) that shows preferential antitumor activity in *ATM*-deficient cells. **A,** Chemical structure of ART0380. **B,** ATR-ATRIP Caliper Assay; $n = 3$ independent experiments. **C,** Cellular assays to assess pChk1 (left) and pRPS6 (right) inhibition in HT-29 cells treated with ART0380: EC_{50} curves are shown; $n = 3$ independent experiments. **D,** Representative growth curves for the *in vitro* cellular proliferation inhibitory potency of ART0380 in NCH-H23, Granta-519, LoVo, and CCD-18Co cells treated with ART0380 for 7 days and average EC_{50} values (μmol/L) of the indicated cancer cell lines; $n = 3$ independent experiments. **E,** Growth curves of parental or *ATM* KO isogenic NCI-H460, Calu-6, and PC-3 cells treated with a dose titration of ART0380 for 7–10 days. EC_{50} values (μmol/L) of cancer cell lines are the average of at least 2 technical replicates. **F,** Cell-cycle profile of *ATM* KO and parental NCI-H460 cells treated with a dose titration of ART0380 for 48 hours or 24 hours on/24 hours off. **G,** Evaluation of γH2AX foci accumulation in geminin-positive *ATM* KO and parental NCI-H460 (H460-P) cells treated with a dose titration of ART0380 for 48 hours or 24 hours on/24 hours off.

ATR-ATRIP complex enzyme activity, with an IC_{50} of 51.7 ± 14.2 nmol/L (**Fig. 1B**). Using HT-29 colorectal adenocarcinoma cells, cellular activity was assessed by measuring inhibition of ATR-dependent phosphorylation of the downstream target, Chk1 (CHEK1) kinase, at serine 345 (pChk1ser345), and cellular selectivity was demonstrated by measuring the cellular inhibition of the mTor complex *in vitro*. We found that treatment with ART0380 resulted in robust inhibition of pChk1ser345, with EC_{50} in the low nanomolar

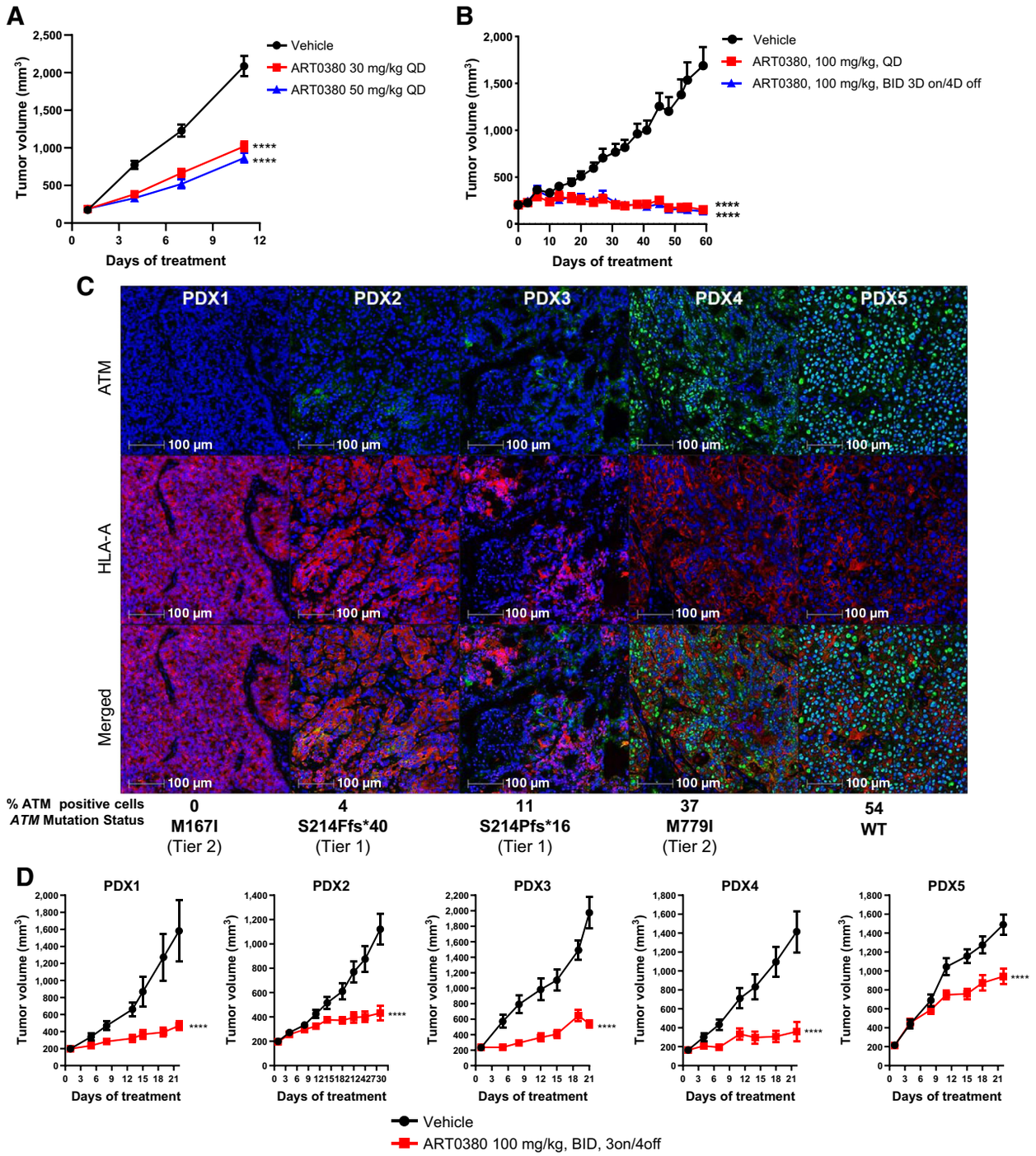

Figure 2.

In vivo antitumor activity of ART0380 in *ATM*-aberrant models. **A,** Tumor growth curve (mm^3) of Granta-519 xenografts, a mantle cell lymphoma cell line with known *ATM* missense mutation and low ATM protein expression, treated with ART0380 at 30 and 50 mg/kg, qd. Data are presented as the mean ± SEM and *P* values are calculated by two-way ANOVA with multiple comparisons and Tukey correction, compared with vehicle control (****, $P < 0.0001$; $n = 10$ mice/group). **B,** Tumor growth curve (mm^3) of *ATM*-deficient non–small cell lung cancer patient–derived xenograft (PDX) model treated with ART0380 at 100 mg/kg qd and 100 mg/kg b.i.d., 3 days on/4 days off. Data are presented as the mean ± SEM, and *P* values are calculated by two-way ANOVA with multiple comparisons and Tukey correction, compared with vehicle control (****, $P < 0.0001$; $n = 10$ mice/group). **C,** Evaluation of ATM expression by immunofluorescence across tumor sections of indicated colorectal PDX models (ATM: green; HLA-A: red; DAPI: blue; scale bar 100 µm). The total number of positive cells determined by nuclear expression of ATM in the tumor as well as *ATM* variant status is listed. Tier 1: protein-altering, deleterious variants; Tier 2: VUS, benign variants. **D,** Tumor growth curve (mm^3) of indicated colorectal cancer (CRC) PDX models treated with ART0380 100 mg/kg b.i.d. with a 3 days on/4 days off dosing regimen. Data are presented as the mean ± SEM, and *P* values are calculated by two-way ANOVA with multiple comparisons and Sidak correction, compared with vehicle control (****, $P < 0.0001$; $n = 10$ mice/group).

range, suggesting potent cellular activity. On the contrary, inhibition of the mTor complex was minimal, with EC_{50} in the micromolar range (**Fig. 1C**). Inhibition of downstream markers of the ATR-related enzymes ATM, DNA-PKcs (PRKDC), mTOR (MTOR), and SMG1 was studied in response to DNA damage induced by etoposide in NCI-H460 cells with no inhibition observed at a top concentration of 3 μmol/L (Supplementary Fig. S1A), suggesting a good range of selectivity in cells over PIKK-related proteins.

Phenotypic response to ART0380 was evaluated on a selected cell line panel that included two *ATM* LOF cell lines, NCI-H23 (34) and Granta 519 (35), as well as the LoVo cell line, a colorectal adenocarcinoma model with high baseline levels of replication stress (36), and

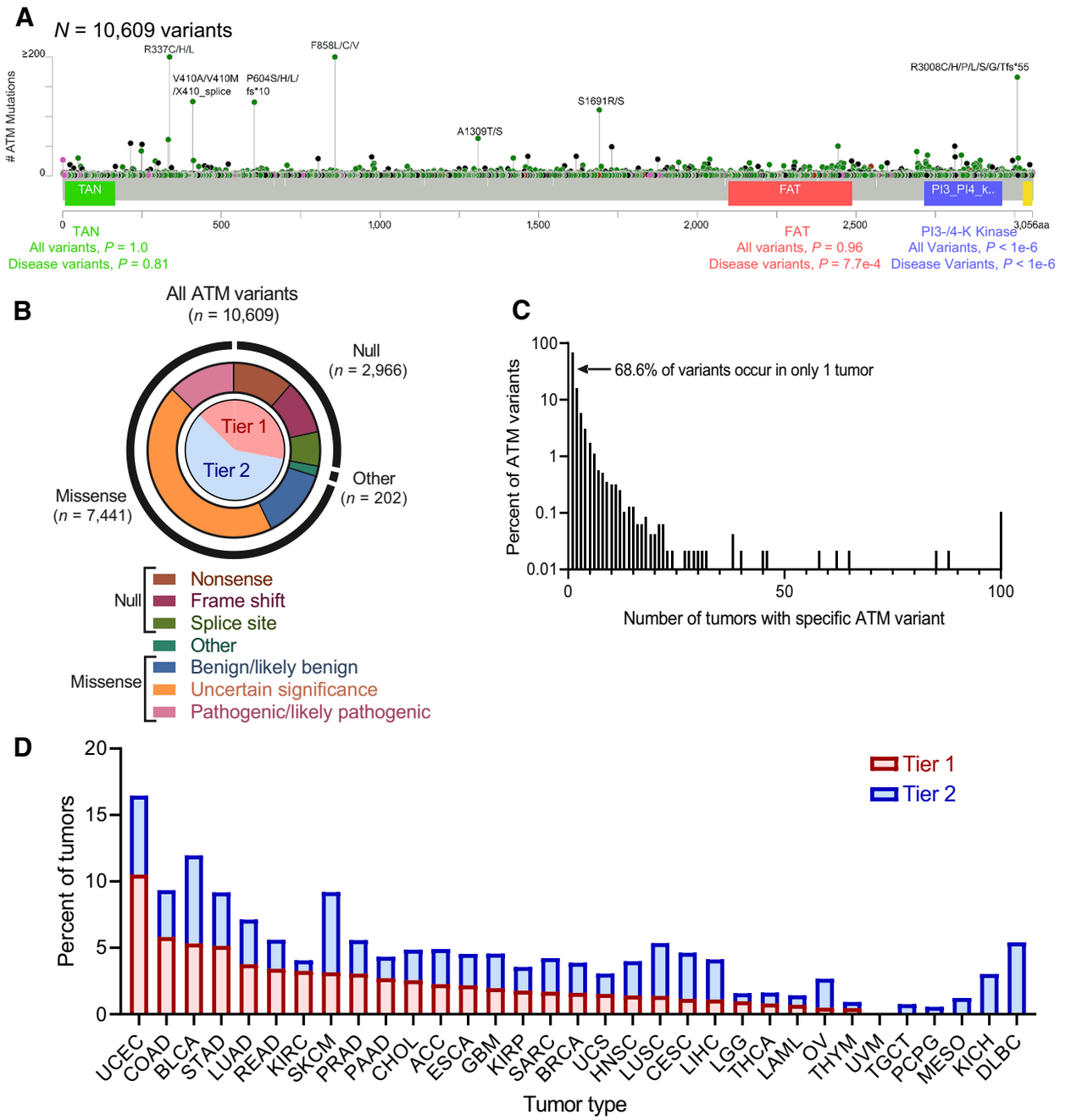

Figure 3.

Pan-cancer landscape of *ATM* variants. Tier 1 *ATM* variants are protein-altering, deleterious variants; Tier 2 *ATM* variants are VUS, benign. **A** and **B,** Variants in *ATM* span the entirety of the exonic portion of the gene, with the majority being VUS or benign missense variants. Functional kinase domains were significantly more likely to have disease-causing missense variants. **C,** The majority of variants occur in only a single patient. Relatively few variants occur in more than 100 individuals (hotspots). **D,** The ratio of Tier 1 to Tier 2 variants, defined in **A** and **B**, differs by tumor type. (*Continued on the following page.*)

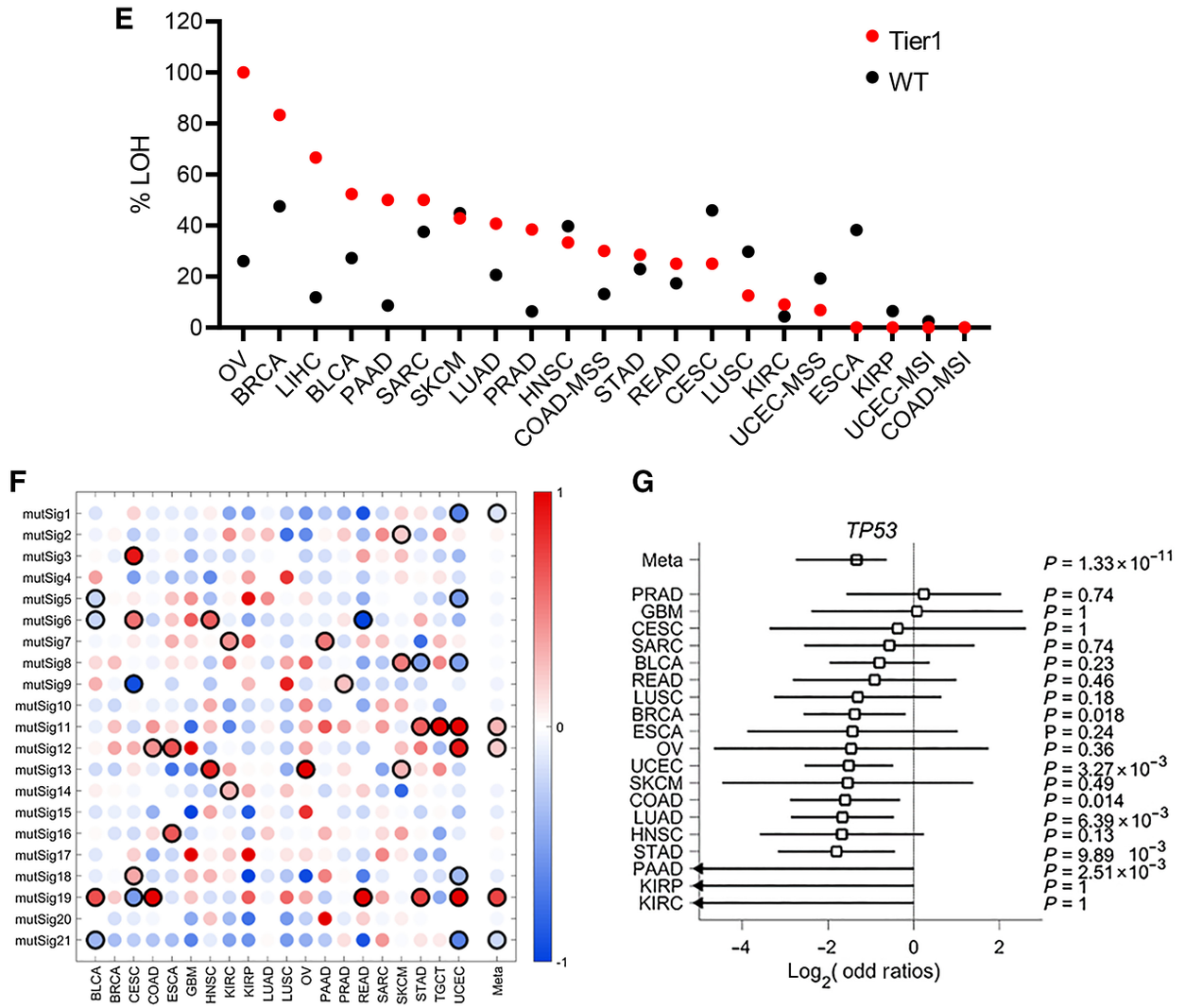

Figure 3.

(*Continued.*) **E,** Selective pressure for loss of heterozygosity (LOH) by tumor type in tumors with Tier 1 variants versus *ATM*-wild-type. **F,** Mutational signatures of tumors with Tier 1 variants differ by tissue of origin. **G,** Co-occurrence of deleterious variants in *ATM* and *TP53* differ by tumor type and are mutually exclusive in pan-cancer meta-analysis.

the CCD-18Co cell line, a normal colon fibroblast model. ART0380 induced robust inhibition of cell growth, particularly in the two ATM LOF cell lines, whereas only minimal response was observed in CCD-18Co normal fibroblasts (**Fig. 1D**).

Selective sensitivity to ART0380-induced ATR inhibition in cells with *ATM* loss was confirmed in NCI-H460 (lung cancer), Calu-6 (lung cancer), and PC-3 (prostate cancer) isogenic cells with *ATM* knockout (*ATM* KO), wherein a more robust response was observed from *ATM* KO cells than from parental ATM wild-type cells (**Fig. 1E**; Supplementary Fig. S1B). Further evaluation of the NCI-H460 isogenic pairs revealed an increase in apoptosis, as measured by Annexin V/PI staining, in the *ATM* KO cells compared with the parental cells after 48 hours of incubation with ART0380 (Supplementary Fig. S1C).

Cell-cycle analysis and DNA damage accumulation were also assessed in *ATM* KO and WT isogenic NCI-H460 cell lines. Continuous and washout treatments were performed to elucidate the cellular response to ART0380 using different dosing schedules. Inhibiting ATR for 48 hours in *ATM*-proficient cells resulted in the accumulation of cells in G_1-phase with a concomitant decrease of those in S-phase (**Fig. 1F**). These changes were reduced in the ATM-null cells. Using the intermittent ART0380 dosing schedule of 24 hours of treatment followed by 24 hours of incubation without the drug, the cell-cycle changes in the parental cells were similar to those observed with continuous dosing. However, the use of this intermittent regimen in the *ATM* KO cells restored ATR activity (Supplementary Fig. S1D); this, in turn, impaired DNA replication, as evidenced by the accumulation of cells with intermediate DNA content that were unable to incorporate EdU (arrested S-phase) as well as by the reduction in actively replicating cells (**Fig. 1F**). There was also evidence of an accumulation of cells in G_2 phase (**Fig. 1F**) as well as an accumulation of γH2AX

foci in geminin (GMNN)-positive cells, indicating higher levels of DNA damage in the *ATM* KO cells (**Fig. 1G**). These findings were confirmed by Western blotting analysis of downstream DDR markers (Supplementary Fig. S1D). Together, our data suggest that ART0380 potently impairs cell cycle and specifically increases DNA damage in ATM KO cancer cells exposed to an intermittent treatment schedule, thus suggesting that intermittent dosing along with continuous regimens should be evaluated in future clinical studies.

ART0380 is effective *in vivo* in cancers with varying types of ATM

To assess the antitumor efficacy of ART0380 in ATM LOF tumors *in vivo*, mice bearing LoVo cell xenografts were randomized into groups that received either vehicle control or daily (QD), oral (PO) doses of ART0380 of 10, 30, 50, or 100 mg/kg. ART0380 was found to be well tolerated over the course of the study (Supplementary Fig. S2A). Further, ART0380 treatment induced significant tumor growth inhibition in a dose-dependent manner, with doses of 30 mg/kg inducing an antitumor response comparable with the clinical benchmark AZD6738, and doses of 50 mg/kg and 100 mg/kg further increasing the percentage of tumor growth inhibition to 84 and 96 ($P < 0.0001$), respectively (Supplementary Fig. S2B). ART0380 was also confirmed to specifically target ATR kinase signaling *in vivo*, as evidenced by Western blot analysis showing modulation of pChk1 Ser345 in tumor xenograft tissues upon ART0380 treatment following induction of DNA damage and replication stress with gemcitabine (Supplementary Fig. S2C). In mice bearing ATM LOF Granta-519 xenografts, tumor growth inhibition was observed in groups treated with either 30 or 50 mg/kg ART0380 when compared with that in vehicle-treated mice (**Fig. 2A**; Supplementary Fig. S3A). Additionally, tumor regression was observed upon treatment with 100 mg/kg ART0380 on QD or intermittent dosing schedules in a lung adenocarcinoma PDX model harboring a deleterious *ATM* gene variant (p.E473*), which induced a near total loss of ATM protein (**Fig. 2B**; Supplementary Fig. S3B and S3C).

Given the heterogeneity in response observed from patients with *ATM* LOF cancers during ATR inhibitor trials thus far, we assessed the effectiveness of ART0380 against a panel of colorectal cancer PDX models that harbored varying degrees of ATM protein expression and differing *ATM* variant status (**Fig. 2C**). Our findings demonstrate that ART0380 treatment resulted in tumor growth inhibition in PDX1, which harbored total ATM LOP and a missense variant in *ATM*, as well as in PDX2 with a deleterious variant and near complete ATM LOP (**Fig. 2D**; Supplementary Fig. S3D). In addition, antitumor efficacy was seen in PDX3 and PDX4, which harbored a frameshift and a missense *ATM* variant, respectively, but retained some ATM protein expression (**Fig. 2C** and **D**). In contrast, ART0380 had the least impact on PDX5, which was confirmed wild-type for *ATM* and retained ATM protein expression (**Fig. 2C** and **D**). Similarly, treatment with the ATR kinase inhibitor tool compound, IACS-030106, resulted in heterogeneous antitumor efficacy across colorectal PDX models with differing types of *ATM* LOF (Supplementary Fig. S4).

Pan-cancer landscape of DNA variants in *ATM* displays tissue-specific variability

To better understand the heterogeneity in response of *ATM* LOF cancers to select anticancer therapies available in the clinic, we first defined the mutational landscape of *ATM* LOF in a tissue-specific context across cancer subtypes. Through comprehensive evaluation of both internal and *in silico* data, we identified 10,609 *ATM* variants in 8,587 individuals with cancer, which is the largest and most diverse set of *ATM*-mutant cancers to date (Supplementary Fig. S6). Variant mapping and annotation revealed that variants spanned across the *ATM* coding sequence, with the majority (70%) identified as missense variants (**Fig. 3A** and **B**). The majority of *ATM* variants (68.6%) were found to be unique to a single individual, with the remainder shared between ≥2 individuals (**Fig. 3C**), highlighting that "hotspot" mutations in *ATM* are relatively rare. With respect to functional impact, 28% ($N = 2{,}966$) were deleterious variants (Tier 1 variants), but the majority of variants (57%) were missense VUS or benign/likely benign (Tier 2 variants, $N = 6{,}090$; **Fig. 3B**). The functional kinase domains of the gene were significantly more likely to have deleterious, known disease-associated missense variants ($P < 0.001$; **Fig. 3A**), which is consistent with a previously published data set that assessed 286 *ATM*-mutant cancers from TCGA database (37).

Variability was observed in the absolute frequency of *ATM* variants, as well as in the proportion of Tier 1 to Tier 2 variant type by tumor lineage (**Fig. 3D**). We assessed whether selective pressure for LOH and targetability for *ATM* mutations were tissue specific, as this has been shown previously for *BRCA1/2*-mutant cancers (23). Our findings show that the correlation between deleterious variants and selective pressure for LOH differed by tissue type (**Fig. 3E**). To further assess the functionality of ATM mutations across cancer types, we assess the relative prevalence of different hallmark mutational signatures that reflect a variety of known mutational processes such as mismatch-repair defects, smoking, UV DNA damage, homologous recombination repair defects, as well as unknown mutational processes (32). Additionally, mutational signatures enriched in tumors with Tier 1 *ATM* variants differed widely by tissue type, with pan-cancer meta-analysis revealing a positive correlation between tissue of origin and mutSig19, mutSig11, and mutSig12 in tumors with Tier 1 *ATM* variants (**Fig. 3F**). Notably, with very few exceptions, tumors with Tier 1 *ATM* variants did not harbor an overall enrichment of mutSig3, a signature associated with defective homologous recombination repair and enriched in studies in tumors with loss of *BRCA1/2* (38).

The TP53 signaling pathway, which contributes to mediating antiproliferative and apoptosis pathways, is activated in part by the ATM kinase in response to cellular stress. Preclinical data using various cancer subtypes have shown that *TP53* mutation status can affect the vulnerability of *ATM*-depleted cells to genotoxic stress and DNA breaks (39, 40). In addition, mutations in *ATM* and *TP53* have been shown to be mutually exclusive in certain malignancies (41). Accordingly, our pan-cancer meta-analysis of tumors with Tier 1 *ATM* variants confirmed that the majority of tumor types display mutual exclusivity with mutations in *TP53*, although tissue-specific differences are observed (**Fig. 3G**).

Paired DNA sequencing and protein staining identify tumors with ATM loss

To better define the relationship between *ATM* variants, ATM protein loss, and clinical outcomes, IHC analysis for ATM protein expression was performed on 480 patient tumors with available *ATM* sequencing data, with 471/480 patient tumors with interpretable IHC results (**Fig. 4A**). Tumors with null, inactivating variants in *ATM* were significantly more likely to display ATM LOP than tumors with missense variants ($P = 5.8e^{-9}$) or *ATM*-wild-type ($P = 1.8e^{-14}$), although 19% ($N = 27/140$) and 9% ($N = 13/149$) of tumors with *ATM-VUS* and *ATM-wild-type*, respectively, showed ATM LOP (**Fig. 4B**). IHC analysis of ATM expression also found that 145 patient

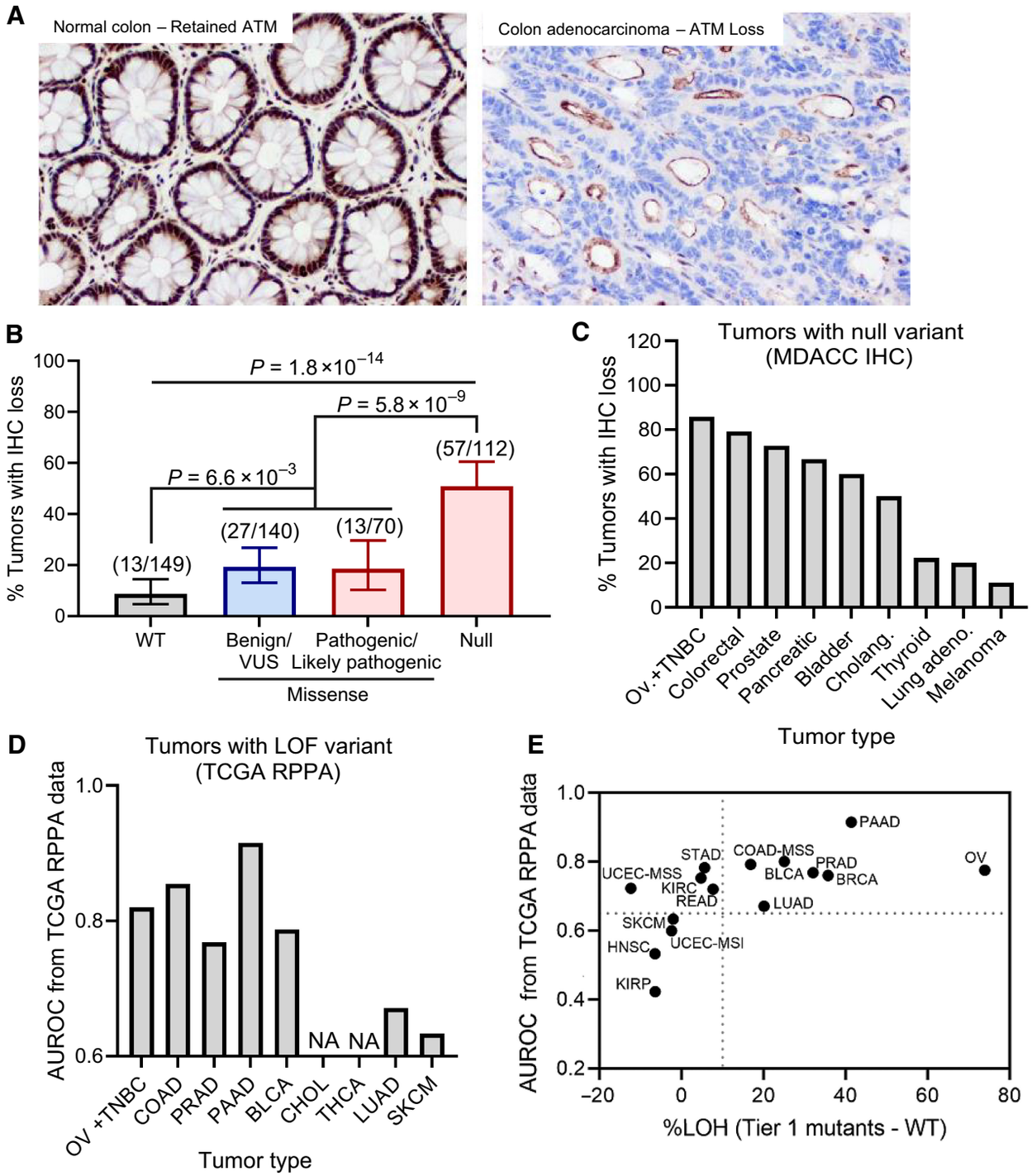

Figure 4.

Relationship between *ATM* variant status and ATM protein expression. **A,** Example images of ATM IHC staining showing retained protein expression in normal colon tissue (left) vs. loss of protein (LOP) in colon adenocarcinoma (right) using ATM clone Y170 antibody. LOP is defined as 100% loss of staining in tumor cell nuclei. **B,** Association between complete LOP (y axis) and ATM variant status (x axis) in $N = 471$ patient tumors. **C** and **D,** The relationship of LOP (y axis; C) and tumors with known deleterious, null variants (D) is variable by tissue type. **E,** Correlation of ATM LOP and ATM loss of heterozygosity (LOH) in tumors with Tier 1 *ATM* variants (protein-altering, deleterious variants) across tumor tissue type.

tumors presented with shared variant(s) in *ATM,* with variant-to-IHC results revealing an 84.8% consistency across tumors, but disparate variant-to-IHC results were observed across several tumor types. For example, of the five tumors harboring the deleterious *R1730** variant in *ATM*, the three tumors with full ATM protein expression were all melanomas, whereas the two tumors harboring ATM LOP were both colorectal adenocarcinomas.

To further explore this potential dependence of ATM LOP on tumor type, we analyzed the association between null, protein-truncating variant(s) in *ATM* and ATM LOP across different tumor types using IHC analysis. We found that ATM LOP was prevalent in colorectal, HBOC subtypes (breast, ovarian), prostate, and pancreas tumors harboring null *ATM* variants, but less prevalent in lung cancer and melanoma with null *ATM* variants (**Fig. 4C**). This observation was further validated in patient tumors from TCGA, where ATM LOP, as measured by reverse phase protein array (RPPA), robustly identified null ATM variants in colorectal, breast, ovarian, prostate, and pancreas cancers but did not in lung cancer and melanoma (**Fig. 4D**). These results suggest that the correlation between deleterious variants in the *ATM* gene and the resultant ATM LOP phenotype may differ by cancer subtype and may be indicative of subclonal events specific to certain tumor types. It is also noted that tumors with Tier 1 variants in *ATM* with a stronger correlation with ATM LOP also correlated with LOH of the second allele across most tumor types (**Fig. 4E**).

With these aforementioned novel findings on variant and tissue specificity in ATM LOF, we then evaluated the predictive capacity of ATM LOF in this context using retrospective treatment data from patients with advanced solid malignancies. First, we performed a retrospective clinical chart review of patients with *ATM*-mutant cancers and identified 77 patients (51 prostate, pancreatic, breast, and ovarian cancers; 15 colorectal cancers; 11 cholangiocarcinomas) with IHC analyses and clinical DNA sequencing data who had received platinum-based chemotherapy in the metastatic setting with available follow-up data. We found that patients whose tumors harbored *ATM* Tier 1 variants and ATM LOP had significantly better PFS when compared with patients whose tumors harbored *ATM*-wild-type or -*VUS* and were without protein loss (HR, 0.50; 95% CI, 0.28–0.89, $P = 0.03$, log-rank test; **Fig. 5A**). Importantly these platinum-treated samples included more penetrant tumor types that show a stronger correlation with *ATM* Tier 1 variants, LOH, and ATM LOP (**Fig. 4E**). These findings were confirmed using a Cox proportional hazards model with tumor type as a stratification variable (**Fig. 5B**).

Early-phase clinical trials show ATR kinase inhibitors to be safe as well as demonstrate promising efficacy in patients with advanced cancers with *ATM* LOF, including responses in patients with deleterious *ATM* gene variants but with retained ATM protein, and from patients with complete loss of ATM protein but no identified *ATM* gene variant (17, 18). However, expansion studies have yielded mixed response rates in patients with advanced ATM *LOF* cancers, even within subgroups harboring the same *ATM* variant (18, 20–22). To better understand this heterogeneity, we retrospectively analyzed the *ATM* variant type under the context of tissue specificity and how this affected efficacy in 43 patients treated on phase I/II single-agent ATR inhibitor trials. Of note, patients who harbored *ATM* Tier 1 variants that were strongly correlated with LOH and ATM LOP were defined as class I (penetrant tumor type), whereas patients with tumor types with *ATM* Tier 1 variants that did not strongly correlate with LOH and ATM LOP were categorized as class II (nonpenetrant tumor type). Our findings show that class I patients demonstrated greater clinical benefit rate [10/37(27%) vs. 0/6 (0%)], which was defined as stable disease (SD) or better for greater than 180 days, as well as improved PFS [(HR, 0.48; $P = 0.08$) when compared with class II patients; **Fig. 5C**; Supplementary Fig. S5A]. This phenomenon was more pronounced when controlling for cancers with poor baseline prognosis, including pancreatic cancer and *KRAS*-mutant colorectal cancer (Supplementary Fig. S5B; ref. 42). Of note, our analyses included patients harboring heterogeneous tumor types, with most patients having been heavily pretreated in the metastatic setting. In addition, the trials allowed for ATM defects identified by various platforms, including liquid biopsy. Interestingly, only 1/8 of patients with a Tier 1 *ATM* variant (ATM K2710*), as discovered by a liquid biopsy platform, displayed clinical benefit. Because many liquid biopsy platforms lack a normal DNA control, these *ATM* variants may be associated with clonal hematopoiesis of indeterminate potential (CHIP; ref. 43). Thus, it is important to consider this when deciding on which liquid and tissue platforms to utilize when evaluating for ATM mutations and also stressed the importance of a normal DNA control.

Overall, our studies highlight the importance of further refining how different *ATM* variants may influence protein expression, ATM function, and treatment response in tissue-specific contexts. Specifically, our analysis indicates that, even for *bona fide ATM* deleterious mutations, functional effects may be most relevant in penetrant, class I tumor types, such as breast, ovarian, prostate, pancreatic, and colorectal cancers with microsatellite stability. By contrast, the functional effects of ATM LOF may be relatively less relevant in nonpenetrant, class II tumor types such as melanoma, endometrial, and kidney cancers. Further, the genomic sequencing platform, variant origin (germline vs. somatic), and co-occurrence of additional strong prognostic biomarkers (e.g., *KRAS* mutations in colorectal cancer) may influence treatment response to targeted therapies. Thus, we present a novel algorithm that is readily implementable in clinical settings for utilizing *ATM* LOF as a predictive biomarker (**Fig. 5D**), and this approach will be validated in ongoing prospective clinical trials.

Discussion

ATM is a tumor suppressor involved in mediating pathways affecting cancer cell survival and proliferation, and aberrations resulting in *ATM* LOF have been observed across multiple cancers. Accordingly, efforts have been made to leverage targeted therapies, including ATRi and PARPi, to treat tumors harboring ATM LOF, but significant heterogeneity in response to treatment has been observed in the clinic despite strong preclinical evidence. Therefore, identifying the optimal biomarker of ATM LOF in cancer as well as defining the phenotype of ATM LOF tumors is imperative to guiding targeted therapy selection, interpreting clinical trial results, and improving patient outcomes.

Here, we disclose a novel, potent, and selective ATR inhibitor, ART0380, with nanomolar activity against the ATR/ATRIP complex and a good selectivity window (**Fig. 1**). Consistent with preclinical data and clinical observations of ATR inhibitors as a class, cells harboring ATM LOF as well as PDX models harboring varying degrees of *ATM* LOF were selectively sensitive to ART0380 treatment. Importantly, response to ART0380 was seen in colorectal PDX models with differing types of *ATM* variants and degrees of protein loss (**Fig. 2**). These preclinical data further supported the biological rationale for the clinical evaluation of ART0380 in the context of patients with ATM aberrations but also revealed that potentially targetable *ATM* LOF tumors can display a spectrum of genomic and proteomic defects in ATM. Accordingly, we have launched an active phase I clinical trial testing the efficacy of ART0380 alone or in combination in patients with advanced cancer (NCT04657068). Patient samples from this

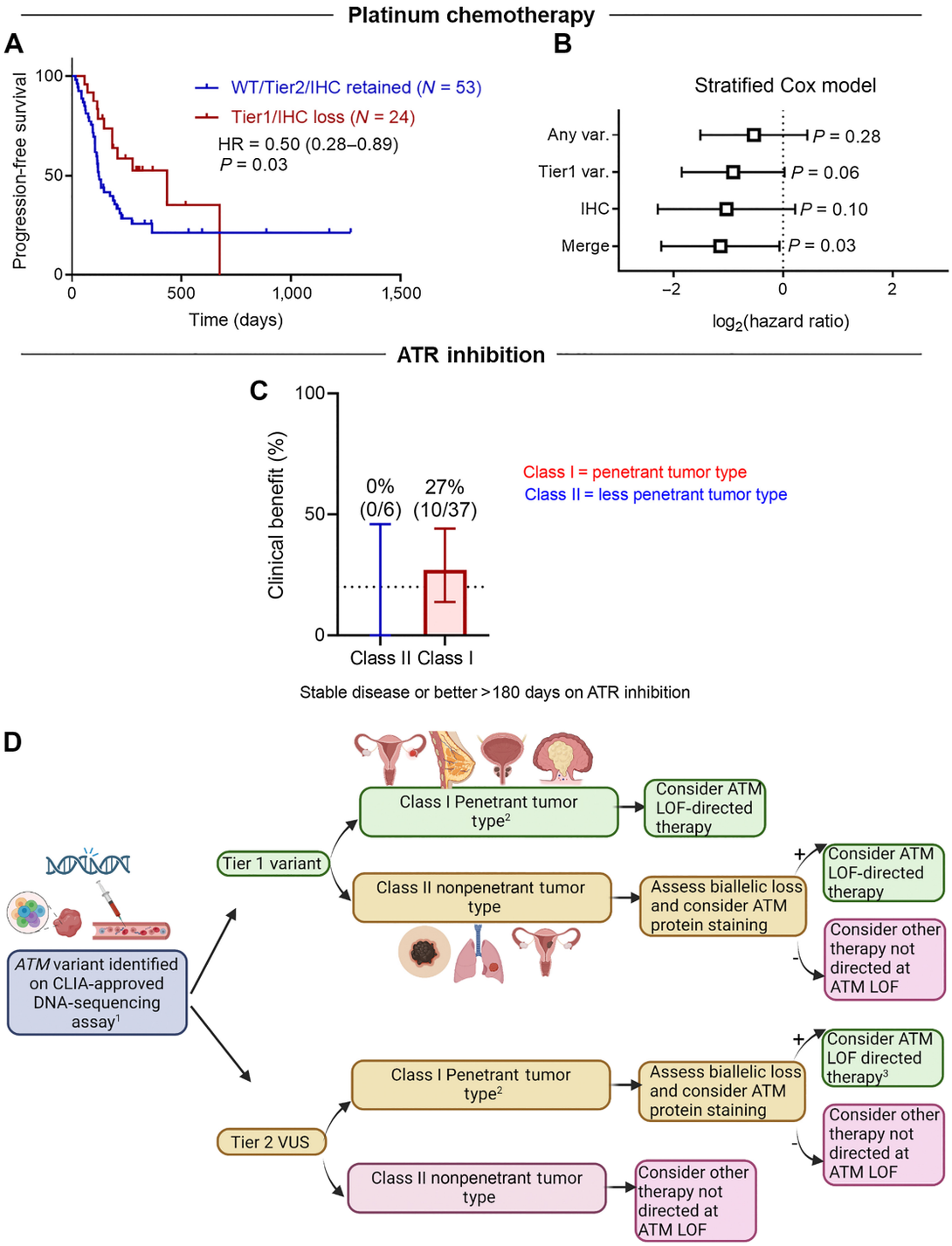

[1]Germline or somatic variant in ATM identified on next generation sequencing with matched normal control. [2]Penetrant tumor type examples include ovary, breast, prostate, MSS colorectal, pancreas, gastric; non penetrant tumor type examples include melanoma, NSCLC, endometrial. [3]Biallelic loss of *ATM* confirms loss of function with loss of protein staining providing added confidence.

Figure 5.

Variant and tissue specificity in targeting ATM loss of function (LOF). **A,** Progression-free survival (PFS) of patients with advanced cancer with penetrant tumor types with ATM LOF as well as patients without ATM LOF when treated with platinum chemotherapy. **B,** Stratified Cox proportional hazards model showing significance when both variant and protein staining are considered (right). **C,** Clinical benefit of ATRi treatment experienced by patients with advanced cancer with Tier 1 ATM variants and more (class I) or less (class II) penetrant tumor. Clinical benefit is defined as stable disease or better for greater than 180 days. **D,** Proposed clinical flow of ATM LOF predictive biomarker.

clinical study will be used to further explore the impact of tissue type, variant type, as well as allelic and protein status of ATM to help inform biomarker development.

Heterogeneity in response has limited the efficacy of targeted therapies, such as DNA-damaging chemotherapies, radiation, and DDR inhibitors, against cancers harboring *ATM* LOF. Due to the fact that ATM kinase dysfunction affects multiple downstream pathways that mediate cell survival and proliferation, as well as the prevalence of *ATM* LOF across cancer types, ATM aberrations have the potential to be exploited for biomarker development, although efforts to do so have yet to be clinically successful in a pan-cancer fashion. Here, we begin elucidating the factors linking specific ATM aberrations to clinical outcomes. We performed the largest and most comprehensive pan-cancer study of *ATM* aberrations to date and showed that variants in the *ATM* gene are found across the entirety of the coding sequence and across cancer types, with the majority of variants identified as missense variants and unique to a single individual with cancer (**Fig. 3**). Notably, we identified "hotspots" for *ATM* variants shared between patients, which have not been previously well described. Furthermore, we showed that the kinase domain of the gene was significantly more likely to have disease-associated missense variants with a known deleterious impact on the associated ATM protein function, which is consistent with an analysis of *ATM* missense mutations in TCGA (37).

Interestingly, recent synthetic lethal drug screens have revealed that the mode of ATM kinase modulation, whether through specific pharmacologic inhibition, or genetic suppression of ATM protein, influences drug sensitivity (8, 44). For example, although pharmacologic ATM kinase inhibition, but not *ATM* knockout, sensitized cells to PARPi, both ATM inhibition and *ATM* knockout sensitized cells to ATRi, with greater sensitization induced by the ATM kinase inhibitor (44). Thus, our findings suggest that the specific location of a variant and its resultant impact on ATM kinase function may affect drug sensitivity more than the loss of total ATM protein.

Recent emerging evidence suggests that variant tissue of origin may affect the antitumor efficacy of DDR inhibitors, thus complicating efforts to leverage DDR gene aberrations as predictive biomarkers (23). Here, pan-cancer analysis revealed the presence of cancer subtype tissue-specific differences, specifically in (1) the type and prevalence of *ATM* variants (null and/or inactivating variants and deleterious missense variants versus VUS and benign missense variants), (2) the selective pressure for LOH of second allele, and (3) the genomic signatures of tumors with deleterious variants in *ATM*. Our data show that, unlike *BRCA1/2*-aberrant tumors, the majority of tumor types with known deleterious *ATM* variants do not display traditional homologous recombination deficient (HRD) signatures (e.g., signature 3), which has been noted in prior genomic studies (32, 38). This, along with the fact that *ATM* LOF does not result in the same degree of HRD or *BRCAness* phenotypes as deleterious mutations in *BRCA1/2*, may help explain why *ATM* aberrancy has yielded inconsistent results as a predictive biomarker for PARPi, which is relatively HRD-specific in single-agent use (8, 16, 32, 45).

Mutations in *ATM* and *TP53* genes have been previously shown to be relatively mutually exclusive in certain cancers, which is consistent with our findings herein with tissue-specific differences (4, 41, 46). Preclinical data have shown that both *ATM* and *TP53* defects may predict sensitivity to ATRi, and TP53 *activity* may influence sensitivity to DNA-damaging and DDR-targeted therapy in *ATM*-aberrant tumors (35, 39). Given this mutual exclusivity of functional defects in these genes, *in silico* tools assessing the resulting impact on protein function of *ATM* variants may be better informed by incorporating *TP53* status as well.

The correlations among deleterious variants in *ATM*, selective pressure for LOH, and loss of ATM protein differed by cancer tissue type. For example, colorectal, HBOC cancer subtypes, prostate, and pancreatic cancers displayed a significantly stronger concordance (77%) between inactivating variants and protein loss than did melanoma and lung adenocarcinoma (16%; **Fig. 4**). Although these differences could be due to issues with antibody staining, we noted that, of the five tumors harboring the *R1730* ATM* variant, the two that displayed a complete loss of ATM protein were both colorectal cancer whereas the three that retained protein expression were all cutaneous melanoma. Tissue specificity for a variant's functional impact has recently been shown for *BRCA1/2* as well, whereby variants in these genes in non-HBOC cancer subtypes (where penetrance of mutations in these genes is low) have been shown to be not phenotypically meaningful and selective pressure for LOH to be not pronounced. Instead, variants in *BRCA1/2* in non-HBOC cancer subtypes were likely acting as passenger events, and thus were not actionable for targeted treatment with PARPi (23). Similarly, our findings suggest that *ATM* variants are likely subclonal in certain cancer types and may not necessarily be driver events in a pan-cancer fashion. Furthermore, the tissue specificity for penetrance of *ATM* LOF has the potential to help shape trial design and treatment selection for patients with *ATM*-aberrant cancers (**Fig. 5**).

Our findings revealed that tumors with deleterious, inactivating *ATM* variants were significantly more likely to display complete loss of protein, likely because these variant types affected protein structure and degradation. However, we identified patients harboring tumors with known deleterious variants and retained ATM protein expression, as well as patients who displayed complete loss of ATM protein despite no identifiable inactivating *ATM* variant, which included 9% of patients who were confirmed wild-type for *ATM* (**Fig. 4**). Recent clinical studies found that patients who were wild-type for *ATM* but with complete ATM protein loss did not clinically benefit from ATRi (20, 21), and further studies into coalterations or epigenetic modifiers that affect ATM function are ongoing.

Discrepancies in the clinical definition and diagnostic methods of ATM LOF can complicate efforts to connect ATM variant status and therapeutic outcome. For instance, liquid biopsy platforms are increasingly being used for clinical somatic sequencing and can identify variants in *ATM*. Notably, only a single patient (1/8) with a Tier 1 *ATM* variant identified by liquid biopsy displayed clinical benefit to ATRi greater than 180 days in our analysis of patients with ATM alterations treated with single-agent ATRi. Germline and somatic DNA sequencing using a CLIA-approved platform that includes a normal DNA sample for somatic control and biallelic status, with confirmation by IHC staining, were shown to be the most informative for identifying ATM LOF (**Fig. 5**). A matched normal DNA control to distinguish true cancer-associated targetable *ATM* variants is necessary because *ATM* is among the number of genes where false-positive results may arise from sequencing in the setting of CHIP (43). Liquid biopsy platforms that can delineate these false-positive results are attractive for clinical use given the ease of sampling compared with tissue biopsies, though tissue biopsy currently remains gold standard.

Finally, our retrospective analyses demonstrate that a novel algorithmic approach that incorporates variant type, protein status, and tissue type specificity for *ATM* LOF may be leveraged to predict benefit to select anticancer therapies (**Fig. 5**). We found tissue-specific differences in clinical response to ATRi monotherapy in patients with *ATM* LOF, whereby patients with tumor types harboring Tier 1 variants

strongly correlated with LOH and ATM LOP had greater clinical benefit than those with less penetrant tumor types. Although our current study is limited by the retrospective nature of the clinical data, we are conducting prospective biomarker-selected clinical trials of various targeted and immune-oncology agents in patients with *ATM* LOF (e.g., NCT04266912). Furthermore, there are mechanisms of sensitivity to platinum chemotherapy and ATRi outside of just *ATM* LOF, and there may be other modifiers (e.g., genomic, epigenetic, tumor microenvironment mediated) that alter sensitivity to targeted agents such as ATRi in the clinic.

Early-phase clinical studies of single-agent ATRi have shown promise for patients with *ATM* LOF. For instance, recent clinical data have demonstrated that patients with biallelic loss of the gene, which was strongly correlated with ATM LOP, responded best to ATRi monotherapy (21, 22), which is consistent with our findings. Additionally, studies have also highlighted the importance of combined genomic and proteomic profiling for identifying the maximum number of patients with *ATM* LOF that may benefit from select anticancer therapies, including ATR kinase inhibition (17, 18). Therefore, to refine ATM LOF as a predictive biomarker, it is imperative to further delineate the genotype to phenotype relationship of distinct *ATM* variants, with a particular focus on how tissue specificity, *ATM* variant type, *ATM* biallelic or monoallelic loss, and comutations may influence ATM function and subsequent susceptibility to therapy.

Overall, our findings demonstrate ATM LOF is highly prevalent across several cancer types and is a promising therapeutic target in select patient populations. Synthetic lethal screens of ATM aberrancy and anticancer drugs, including DDR inhibitors, have revealed numerous opportunities for targeting cancers with ATM functional loss, while also elucidating that there may be differences in sensitivity based on the specific type of ATM defect, zygosity, and tumor tissue context.

Data and materials availability

All data are available in the main text or the supplementary materials.

Authors' Disclosures

P.G. Pilié reports personal fees from Janssen Pharmaceuticals outside the submitted work; in addition, P.G. Pilié has a patent for Replication Stress Response Deficiency Gene Signature pending to MD Anderson Cancer Center. V. Giuliani reports other support from Artios Pharma during the conduct of the study. D. Yang reports other support from Astellas Pharma outside the submitted work. K.R. Shaw reports other support from Philips Healthcare outside the submitted work. F. Meric-Bernstam reports personal fees from AbbVie, Aduro BioTech Inc., Alkermes, AstraZeneca, Daiichi Sankyo Co. Ltd., Calibr (a division of Scripps Research), DebioPharm, Ecor1 Capital, eFFECTOR Therapeutics, F. Hoffman-La Roche Ltd., GT Apeiron, Genentech Inc., Harbinger Health, IBM Watson, Incyte, Infinity Pharmaceuticals, Jackson Laboratory, Kolon Life Science, LegoChem Bio, Lengo Therapeutics, Menarini Group, OrigiMed, PACT Pharma, Parexel International, Pfizer Inc., Protai Bio Ltd, Samsung Bioepis, Seattle Genetics Inc., Tallac Therapeutics, Tyra Biosciences, Xencor, Zymeworks, Black Diamond, Biovica, Eisai, FogPharma, Immunomedics, Inflection Biosciences, Karyopharm Therapeutics, Loxo Oncology, Mersana Therapeutics, OnCusp Therapeutics, Puma Biotechnology Inc., Seattle Genetics, Sanofi, Silverback Therapeutics, Spectrum Pharmaceuticals, Theratechnologies, Zentalis, and Dava Oncology; grants from Aileron Therapeutics, Inc., AstraZeneca, Bayer Healthcare Pharmaceutical, Calithera Biosciences Inc., Curis Inc., CytomX Therapeutics Inc., Daiichi Sankyo Co. Ltd., Debiopharm International, eFFECTOR Therapeutics, Genentech Inc., Guardant Health Inc., Klus Pharma, Takeda Pharmaceutical, Novartis, Puma Biotechnology Inc., and Taiho Pharmaceutical Co.; and other support from European Organisation for Research and Treatment of Cancer (EORTC), European Society for Medical Oncology (ESMO), Cholangiocarcinoma Foundation, and Dava Oncology outside the submitted work. C. Liu reports other support from Artios Pharma during the conduct of the study. J.P. Bardenhagen reports other support from Artios Pharma during the conduct of the study. C.P. Vellano reports other support from Artios Pharma during the conduct of the study. J.R. Marszalek reports other support from Artios Pharma outside the submitted work. E. Rajendra reports being an employee and shareholder of Artios Pharma Ltd. D. Piscitello reports being an employee and shareholder of Artios Pharma Ltd. T.I. Johnson reports being an employee and shareholder of Artios Pharma Ltd. M. Likhatcheva reports being an employee and shareholder of Artios Pharma Ltd. E. Elinati reports being an employee and shareholder of Artios Pharma Ltd. J.B. Majithiya reports being an employee and shareholder of Artios Pharma Ltd. J. Neves reports being an employee and shareholder of Artios Pharma Ltd. V. Grinkevich reports being an employee and shareholder of Artios Pharma Ltd. M. Ranzani reports being an employee and shareholder of Artios Pharma Ltd. M.R. Luzarraga reports being an employee and shareholder of Artios Pharma Ltd. M. Boursier reports being a former employee and being a shareholder of Artios Pharma Ltd. L. Armstrong reports being an employee and shareholder of Artios Pharma Ltd. L. Geo reports being an employee and shareholder of Artios Pharma Ltd. G. Lillo reports being an employee and shareholder of Artios Pharma Ltd. W. Tse reports being an employee and shareholder of Artios Pharma Ltd. S. Kopetz reports other support from Lutris, Iylon, Frontier Medicines, Xilis, Navire, Genentech, EMD Serono, Merck, Holy Stone Healthcare, Novartis, Lilly, Boehringer Ingelheim, AstraZeneca/MedImmune, Bayer Health, Redx Pharma, Ipsen, HalioDx, Lutris, Jacobio, Pfizer, Repare Therapeutics, Inivata, GlaxoSmithKline, Jazz Pharmaceuticals, Iylon, Xilis, AbbVie, Amal Therapeutics, Gilead Sciences, Mirati Therapeutics, Flame Biosciences, Servier, Carina Biotech, Bicara Therapeutics, Endeavor BioMedicines, Numab, Johnson & Johnson/Janssen, Genomic Health, Frontier Medicines, Replimune, Taiho Pharmaceutical, Cardiff Oncology, Ono Pharmaceutical, Bristol Myers Squibb-Medarex, Amgen, Tempus, Foundation Medicine, Harbinger Oncology, Takeda, CureTeq, Zentalis, Black Stone Therapeutics, NeoGenomics Laboratories, Accademia Nazionale Di Medicina, Tachyon Therapeutics, Sanofi, Biocartis, Guardant Health, Array BioPharma, Genentech/Roche, EMD Serono, MedImmune, Novartis, Amgen, Lilly, and Daiichi Sankyo outside the submitted work. M. Geck Do reports other support from Artios Pharma during the conduct of the study. S. Lively reports personal fees from Johnson & Johnson outside the submitted work; in addition, S. Lively has patents for US10800774B2, US10421765B2, EP3765008A1, and EP3651768A1, all pending and licensed to Artios Pharma. M.G. Johnson reports patents for WO2019036641 and WO2019014618, both pending to MD Anderson. H.M. Robinson reports patents for WO2021/028644A1, WO2016GB50517 20160229, WO2015118338 (A1), and US2022298587 (A1), all pending, as well as being an employee and shareholder of Artios Pharma Ltd. G.C. Smith reports being an employee and shareholder of Artios Pharma Ltd. as well as a shareholder of AstraZeneca PLC. C.L. Carroll reports other support from Artios Pharma during the conduct of the study; in addition, C.L. Carroll has patents for WO2019014618, US 20190016713, US 20200102296, and US 20210047311, all issued and licensed to Artios Pharma. M.E. Di Francesco reports a patent for WO 2019/014618 licensed to Artios. P. Jones reports grants and other support from Artios during the conduct of the study and grants from Artios outside the submitted work; in addition, P. Jones has a patent for US10894052 issued, licensed, and with royalties paid from Artios. T.P. Heffernan reports other support from Artios Pharma during the conduct of the study and other support from Boehringer Ingelheim, Blueprint Medicines, Taiho Pharma, Schrodinger, Nexo Therapeutics, Psivant Therapeutics, and Cullgen Inc. outside the submitted work. T.A. Yap reports other support from University of Texas MD Anderson Cancer Center and from Seagen during the conduct of the study; personal fees from AbbVie, Adagene, Almac, Aduro, Amphista, Artios, Astex, Athena, Atrin, Avenzo, Avoro, Axiom, Baptist Health Systems, BioCity PharmaBoxer, Bristol Myers Squibb, C4 Therapeutics, Calithera, Cancer Reseach UK, Carrick Therapeutics, Circle Pharma, Clovis, Cybrexa, Daiichi Sankyo, Dark Blue Therapeutics, Diffusion, Duke Street Bio, 858 Therapeutics, EcoR1 Capital, and Ellipses Pharma; grants and personal fees from Acrivon, AstraZeneca, Bayer, Beigene, Blueprint, F-Star, Merck, Sanofi, Tango, EMD Serono, Entos, Genesis Therapeutics, Genmab, Glenmark, GLG, Globe Life Sciences, GSK, Guidepoint, Ideaya Biosciences, Idience, Ignyta, I-Mab, Immunesensor, Impact Therapeutics, Institut Gustave Roussy, Intellisphere, Jansen, Kyn, MEI Pharma, Mereo, Merit, Monte Rosa Therapeutics, Natera, Nested Therapeutics, Nexys, Nimbus, Novocure, Odyssey, OHSU, OncoSec, Ono Pharma, Onxeo, PanAngium Therapeutics, Pegascy, PER, Pfizer, Piper-Sandler, Pliant Therapeutics, Prolynx, Radiopharma Theranostics, Repare, resTORbio, Roche, Ryvu Therapeutics, SAKK, Schrodinger, Servier, Synnovation, Synthis Therapeutics, TCG Crossover, TD2, Terremoto Biosciences, Tessellate Bio, Theragnostics, Terns Pharmaceuticals, Tolremo, Tome, Thryv Therapeutics, Trevarx Biomedical, Varian, Veeva, Versant, Vibliome, Voronoi Inc., Xinthera, Zai Labs, and ZielBio; grants from BioNTech, BMS, Boundless Bio, Clovis, Constellation, Cyteir, Eli Lilly, Forbius, GlaxoSmithKline, Genentech, Haihi,

Insilico Medicine, Ionis, Ipsen, Jounce, Karyopharm, KSQ, Kyowa, Mirati, Novartis, Ribon Therapeutics, Regeneron, Rubius, Scholar Rock, Seattle Genetics, Tesaro, Vivace, and Zenith. No disclosures were reported by the other authors.

Authors' Contributions

P.G. Pilié: Conceptualization, resources, data curation, formal analysis, supervision, funding acquisition, validation, investigation, visualization, methodology, writing–original draft, project administration, writing–review and editing. **V. Giuliani:** Conceptualization, resources, data curation, formal analysis, validation, investigation, visualization, methodology, writing–original draft, project administration, writing–review and editing. **W. Wang:** Data curation, formal analysis, supervision, validation, writing–review and editing. **D.J. McGrail:** Data curation, formal analysis, validation, investigation, methodology, writing–review and editing. **C.A. Bristow:** Data curation, formal analysis. **N.Y. Ngoi:** Data curation. **K. Kyewalabye:** Data curation, formal analysis. **K.M. Wani:** Data curation, formal analysis. **H. Le:** Data curation, formal analysis. **E. Campbell:** Data curation, formal analysis. **N.S. Sanchez:** Data curation. **D. Yang:** Data curation. **J.S. Gheeya:** Data curation, investigation. **R.V. Goswamy:** Data curation. **V. Holla:** Data curation. **K.R. Shaw:** Resources, supervision. **F. Meric-Bernstam:** Resources, supervision, writing–review and editing. **C. Liu:** Data curation. **X. Ma:** Data curation. **N. Feng:** Data curation. **A.A. Machado:** Data curation. **J.P. Bardenhagen:** Data curation. **C.P. Vellano:** Data curation, formal analysis. **J.R. Marszalek:** Data curation, formal analysis. **E. Rajendra:** Resources, data curation, formal analysis. **D. Piscitello:** Resources, data curation, formal analysis. **T.I. Johnson:** Resources, data curation, formal analysis. **M. Likhatcheva:** Resources, data curation, formal analysis. **E. Elinati:** Resources, data curation, formal analysis. **J. Majithiya:** Resources, data curation, formal analysis. **J. Neves:** Resources, data curation, formal analysis. **V. Grinkevich:** Resources, data curation, formal analysis. **M. Ranzani:** Resources, data curation, formal analysis. **M. Roy-Luzarraga:** Resources, data curation, formal analysis. **M. Boursier:** Data curation. **L. Armstrong:** Resources, data curation, formal analysis, supervision, investigation, writing–review and editing. **L. Geo:** Resources, data curation, investigation. **G. Lillo:** Resources, data curation, formal analysis, supervision, investigation. **W. Tse:** Resources, data curation, formal analysis, investigation. **A.J. Lazar:** Resources, data curation, formal analysis, supervision, writing–review and editing. **S.E. Kopetz:** Resources, data curation, formal analysis, supervision. **M.K. Geck Do:** Resources, data curation, formal analysis, supervision, writing–review and editing. **S. Lively:** Resources, data curation, formal analysis, supervision. **M.G. Johnson:** Conceptualization, resources, data curation, formal analysis, supervision, investigation, methodology, project administration, writing–review and editing. **H.M. Robinson:** Conceptualization, resources, data curation, formal analysis, supervision, investigation, methodology, project administration, writing–review and editing. **G.C. Smith:** Conceptualization, resources, data curation, formal analysis, supervision, funding acquisition, validation, investigation, visualization, methodology, writing–original draft, project administration, writing–review and editing. **C.L. Carroll:** Conceptualization, resources, data curation, formal analysis, supervision, funding acquisition, validation, investigation, visualization, methodology, writing–original draft, project administration, writing–review and editing. **M.E. Di Francesco:** Conceptualization, resources, data curation, formal analysis, supervision, investigation, methodology, project administration, writing–review and editing. **P. Jones:** Conceptualization, resources, data curation, formal analysis, supervision, investigation, methodology, project administration, writing–review and editing. **T.P. Heffernan:** Conceptualization, resources, data curation, formal analysis, supervision, funding acquisition, validation, investigation, visualization, methodology, writing–original draft, project administration, writing–review and editing. **T.A. Yap:** Conceptualization, resources, data curation, formal analysis, supervision, funding acquisition, validation, investigation, visualization, methodology, writing–original draft, project administration, writing–review and editing.

Acknowledgments

We would like to acknowledge the patients and their families for participating in this research.

This work is supported in part by NIH/NCI Support grant NIH/NCI P30 CA016672 to the University of Texas MD Anderson Cancer Center; Cancer Prevention Research Institute of Texas (CPRIT) Precision Oncology Decision Support Core grant RP150535; Sheikh Khalifa Bin Zayed Al Nahyan Institute for Personalized Cancer Therapy; NIH/NCI R01-CA255074 (T.A. Yap); US Department of Defense Ovarian Cancer Research Program Clinical Translational Research Award OC200482 (T.A. Yap); US Department of Defense Breast Cancer Research Program Breakthrough Award BC211174 (T.A. Yap); V Foundation Clinical Scholar Program VC2020–001 (T.A. Yap); and ASCO Conquer Cancer Foundation Career Development Award (P.G. Pilie).

Note

Supplementary data for this article are available at Clinical Cancer Research Online (http://clincancerres.aacrjournals.org/).

Received June 15, 2023; revised October 31, 2023; accepted February 21, 2024; published first February 28, 2024.

References

1. Lee J-H, Paull TT. Cellular functions of the protein kinase ATM and their relevance to human disease. Nat Rev Mol Cell Biol 2021;22:796–814.
2. Lavin MF. Ataxia-telangiectasia: from a rare disorder to a paradigm for cell signalling and cancer. Nat Rev Mol Cell Biol 2008;9:759–69.
3. Goldgar DE, Healey S, Dowty JG, Da Silva L, Chen X, Spurdle AB, et al. Rare variants in the ATM gene and risk of breast cancer. Breast Cancer Res 2011;13:R73.
4. Weigelt B, Bi R, Kumar R, Blecua P, Mandelker DL, Geyer FC, et al. The landscape of somatic genetic alterations in breast cancers from ATM germline mutation carriers. J Natl Cancer Inst 2018;110:1030–4.
5. Na R, Zheng SL, Han M, Yu H, Jiang D, Shah S, et al. Germline mutations in ATM and BRCA1/2 distinguish risk for lethal and indolent prostate cancer and are associated with early age at death. Eur Urol 2017;71:740–7.
6. AlDubayan SH, Giannakis M, Moore ND, Han GC, Reardon B, Hamada T, et al. Inherited DNA-repair defects in colorectal cancer. Am J Hum Genet 2018;102:401–14.
7. Nanda N, Roberts NJ. ATM serine/threonine kinase and its role in pancreatic risk. Genes (Basel) 2020 [cited 2021 May 10];11. Available from: https://www.ncbi.nlm.nih.gov/pmc/articles/PMC7017295/
8. Rafiei S, Fitzpatrick K, Liu D, Cai M-Y, Elmarakeby HA, Park J, et al. ATM loss confers greater sensitivity to ATR inhibition than PARP inhibition in prostate cancer. Cancer Res 2020;80:2094–100.
9. Moding EJ, Lee C-L, Castle KD, Oh P, Mao L, Zha S, et al. Atm deletion with dual recombinase technology preferentially radiosensitizes tumor endothelium. J Clin Invest 2014;124:3325–38.
10. Turner NC, Lord CJ, Iorns E, Brough R, Swift S, Elliott R, et al. A synthetic lethal siRNA screen identifying genes mediating sensitivity to a PARP inhibitor. EMBO J 2008;27:1368–77.
11. Sundar R, Miranda S, Rodrigues DN, Chénard-Poirier M, Dolling D, Clarke M, et al. Ataxia telangiectasia mutated protein loss and benefit from oxaliplatin-based chemotherapy in colorectal cancer. Clin Colorectal Cancer 2018;17:280–4.
12. Schmid S, Omlin A, Higano C, Sweeney C, Martinez Chanza N, Mehra N, et al. Activity of platinum-based chemotherapy in patients with advanced prostate cancer with and without DNA repair gene aberrations. JAMA Netw Open 2020;3:e2021692.
13. de Bono J, Mateo J, Fizazi K, Saad F, Shore N, Sandhu S, et al. Olaparib for metastatic castration-resistant prostate cancer. N Engl J Med 2020;382:2091–102.
14. Mateo J, Carreira S, Sandhu S, Miranda S, Mossop H, Perez-Lopez R, et al. DNA-repair defects and olaparib in metastatic prostate cancer. N Engl J Med 2015;373:1697–708.
15. Smith TJ. Olaparib in metastatic castration-resistant prostate cancer. N Engl J Med 2021;384:1175.
16. Abida W, Campbell D, Patnaik A, Shapiro JD, Sautois B, Vogelzang NJ, et al. Non-BRCA DNA damage repair gene alterations and response to the PARP inhibitor rucaparib in metastatic castration-resistant prostate cancer: analysis from the phase II TRITON2 study. Clin Cancer Res 2020;26:2487–96.
17. Yap TA, O'Carrigan B, Penney MS, Lim JS, Brown JS, de Miguel Luken MJ, et al. Phase I trial of first-in-class ATR inhibitor M6620 (VX-970) as monotherapy or

in combination with carboplatin in patients with advanced solid tumors. J Clin Oncol 2020;JCO1902404.
18. Yap TA, Tan DSP, Terbuch A, Caldwell R, Guo C, Goh BC, et al. First-in-human trial of the oral ataxia telangiectasia and RAD3-related (ATR) inhibitor BAY 1895344 in patients with advanced solid tumors. Cancer Discov 2021;11:80–91.
19. Ngoi N, Lin HY, Dumbrava EE, Fu S, Karp DD, Naing A, et al. Baseline predictors of hematological toxicity in patients with advanced cancer treated with ATR inhibitors in phase I/II clinical trials. JCO 2022;40:3111.
20. Yap TA, Tan DS, Stathis A, Shapiro GI, Iwasa S, Joerger M, et al. Abstract CT006: Phase Ib expansion trial of the safety and efficacy of the oral ataxia telangiectasia and Rad3-related (ATR) inhibitor elimusertib in advanced solid tumors with DNA damage response (DDR) defects. Cancer Res 2022;82:CT006.
21. Yap TA, Silverman IM, Fontana E, Lee E, Spigel D, Højgaard M, et al. Abstract CT030: Genomic and pathologic determinants of response to RP-3500, an ataxia telangiectasia and Rad3-related inhibitor (ATRi), in patients (pts) with DNA damage repair (DDR) loss-of-function (LOF) mutant tumors in the Phase 1/2 TRESR trial. Cancer Res 2022;82:CT030.
22. Yap TA, Fontana E, Lee EK, Spigel DR, Højgaard M, Lheureux S, et al. Camonsertib in DNA damage response-deficient advanced solid tumors: phase 1 trial results. Nat Med 2023;29:1400–11.
23. Jonsson P, Bandlamudi C, Cheng ML, Srinivasan P, Chavan SS, Friedman ND, et al. Tumour lineage shapes BRCA-mediated phenotypes. Nature 2019;571:576–9.
24. de Bruijn I, Kundra R, Mastrogiacomo B, Tran TN, Sikina L, Mazor T, et al. Analysis and visualization of longitudinal genomic and clinical data from the AACR project GENIE Biopharma Collaborative in cBioPortal. Cancer Res 2023;83:3861–7.
25. Cerami E, Gao J, Dogrusoz U, Gross BE, Sumer SO, Aksoy BA, et al. The cBio cancer genomics portal: an open platform for exploring multidimensional cancer genomics data. Cancer Discov 2012;2:401–4.
26. Integrative analysis of complex cancer genomics and clinical profiles using the cBioPortal—PubMed. [cited 2024 Jan 25]. Available from: https://pubmed.ncbi.nlm.nih.gov/23550210/
27. Knijnenburg TA, Wang L, Zimmermann MT, Chambwe N, Gao GF, Cherniack AD, et al. Genomic and molecular landscape of DNA damage repair deficiency across the cancer genome atlas. Cell Rep 2018;23:239–54.
28. Li Q, Wang K. InterVar: clinical interpretation of genetic variants by the 2015 ACMG-AMP guidelines. Am J Hum Genet 2017;100:267–80.
29. Richards S, Aziz N, Bale S, Bick D, Das S, Gastier-Foster J, et al. Standards and guidelines for the interpretation of sequence variants: a joint consensus recommendation of the American College of Medical Genetics and Genomics and the Association for Molecular Pathology. Genet Med 2015;17:405–24.
30. Chakravarty D, Gao J, Phillips S, Kundra R, Zhang H, Wang J, et al. OncoKB: a precision oncology knowledge base. JCO Precision Oncology 2017;1–16.
31. Landrum MJ, Lee JM, Benson M, Brown GR, Chao C, Chitipiralla S, et al. ClinVar: improving access to variant interpretations and supporting evidence. Nucleic Acids Res 2018;46:D1062–7.
32. Alexandrov LB, Nik-Zainal S, Wedge DC, Aparicio SAJR, Behjati S, Biankin AV, et al. Signatures of mutational processes in human cancer. Nature 2013;500:415–21.
33. Alexandrov LB, Kim J, Haradhvala NJ, Huang MN, Tian Ng AW, Wu Y, et al. The repertoire of mutational signatures in human cancer. Nature 2020;578:94–101.
34. Vendetti FP, Lau A, Schamus S, Conrads TP, O'Connor MJ, Bakkenist CJ. The orally active and bioavailable ATR kinase inhibitor AZD6738 potentiates the anti-tumor effects of cisplatin to resolve ATM-deficient non–small cell lung cancer *in vivo*. Oncotarget 2015;6:44289–305.
35. Menezes DL, Holt J, Tang Y, Feng J, Barsanti P, Pan Y, et al. A synthetic lethal screen reveals enhanced sensitivity to ATR inhibitor treatment in mantle cell lymphoma with ATM loss-of-function. Mol Cancer Res 2015;13:120–9.
36. Foote KM, Blades K, Cronin A, Fillery S, Guichard SS, Hassall L, et al. Discovery of 4-{4-[(3R)-3-Methylmorpholin-4-yl]-6-[1-(methylsulfonyl)cyclopropyl]pyrimidin-2-yl}-1H-indole (AZ20): a potent and selective inhibitor of ATR protein kinase with monotherapy *in vivo* antitumor activity. J Med Chem 2013;56:2125–38.
37. Yamamoto K, Wang J, Sprinzen L, Xu J, Haddock CJ, Li C, et al. Kinase-dead ATM protein is highly oncogenic and can be preferentially targeted by Topoisomerase I inhibitors. Walter J, editor. eLife 2016;5:e14709.
38. Polak P, Kim J, Braunstein LZ, Tiao G, Karlic R, Rosebrock D, et al. A mutational signature reveals alterations underlying deficient homologous recombination repair in breast cancer. Nat Genet 2017;49:1476–86.
39. Reaper PM, Griffiths MR, Long JM, Charrier J-D, Maccormick S, Charlton PA, et al. Selective killing of ATM- or p53-deficient cancer cells through inhibition of ATR. Nat Chem Biol 2011;7:428–30.
40. Kwok M, Davies N, Agathanggelou A, Smith E, Oldreive C, Petermann E, et al. ATR inhibition induces synthetic lethality and overcomes chemoresistance in TP53- or ATM-defective chronic lymphocytic leukemia cells. Blood 2016;127:582–95.
41. Mareckova A, Malcikova J, Tom N, Pal K, Radova L, Salek D, et al. ATM and TP53 mutations show mutual exclusivity but distinct clinical impact in mantle cell lymphoma patients. Leuk Lymphoma 2019;60:1420–8.
42. Zhu G, Pei L, Xia H, Tang Q, Bi F. Role of oncogenic KRAS in the prognosis, diagnosis and treatment of colorectal cancer. Mol Cancer 2021;20:143.
43. Jensen K, Konnick EQ, Schweizer MT, Sokolova AO, Grivas P, Cheng HH, et al. Association of clonal hematopoiesis in DNA repair genes with prostate cancer plasma cell-free DNA testing interference. JAMA Oncol 2021;7:107–10.
44. Wang C, Tang M, Chen Z, Nie L, Li S, Xiong Y, et al. Genetic vulnerabilities upon inhibition of DNA damage response. Nucleic Acids Res 2021;49:8214–31.
45. Marshall CH, Sokolova AO, McNatty AL, Cheng HH, Eisenberger MA, Bryce AH, et al. Differential response to olaparib treatment among men with metastatic castration-resistant prostate cancer harboring BRCA1 or BRCA2 versus ATM mutations. Eur Urol 2019;76:452–8.
46. Greiner TC, Dasgupta C, Ho VV, Weisenburger DD, Smith LM, Lynch JC, et al. Mutation and genomic deletion status of ataxia telangiectasia mutated (ATM) and p53 confer specific gene-expression profiles in mantle cell lymphoma. Proc Natl Acad Sci U S A 2006;103:2352–7.